Blockage of ATGL-mediated breakdown of lipid droplets in microglia alleviates neuroinflammatory and behavioural responses to lipopolysaccharides

Josephine Louise Robb, Frédérick Boisjoly, Arturo Israel Machuca-Parra, Adeline Coursan, Romane Manceau, Danie Majeur, Demetra Rodaros, Khalil Bouyakdan, Karine Greffard, Jean-François Bilodeau, et al.

Brain, Behavior, and Immunity 123 (2025) 315–333

Contents lists available at ScienceDirect

Brain Behavior and Immunity

journal homepage: www.elsevier.com/locate/ybrbi

Full-length Article

Blockage of ATGL-mediated breakdown of lipid droplets in microglia alleviates neuroinflammatory and behavioural responses to lipopolysaccharides

Josephine Louise Robb [a,b], Frédérick Boisjoly [a,c], Arturo Israel Machuca-Parra [a,b], Adeline Coursan [e], Romane Manceau [a,c], Danie Majeur [a,c], Demetra Rodaros [a], Khalil Bouyakdan [a], Karine Greffard [f], Jean-François Bilodeau [f,g], Anik Forest [h], Caroline Daneault [h], Matthieu Ruiz [d,h], Cyril Laurent [a,c], Nathalie Arbour [a,c], Sophie Layé [e,i], Xavier Fioramonti [e,i], Charlotte Madore [e,i], Stephanie Fulton [a,d,i,1], Thierry Alquier [a,b,i,1,*], Representative of consortium

[a] Centre de Recherche du Centre Hospitalier de l'Université de Montréal (CRCHUM), Université de Montréal, Montréal, QC H3T 1J4, Canada
[b] Département de Médecine, Université de Montréal, Montréal, QC H3T 1J4, Canada
[c] Département de Neurosciences, Université de Montréal, Montréal, QC H3T 1J4, Canada
[d] Département de Nutrition, Université de Montréal, Montréal, QC H3T 1J4, Canada
[e] Université de Bordeaux, INRAE, Bordeaux INP, NutriNeuro, UMR 1286, F-33000 Bordeaux, France
[f] Axe Endocrinologie et Néphrologie, CHU de Québec-Université Laval, Québec, QC G1V 4G2, Canada
[g] Département de Médecine, Faculté de Médecine, Université Laval, Québec, QC, G1K 7P4, Canada
[h] Institut de Cardiologie de Montréal, Plateforme de métabolomique, Montréal, QC H1T1C8, Canada
[i] Food4BrainHealth France-Canada International Research Network, Bordeaux, France

ARTICLE INFO

Keywords:
Adipose triglyceride lipase
Lipid droplet
Microglia
Neuroinflammation
Interleukin-6

ABSTRACT

Lipid droplets (LD) are triglyceride storing organelles that have emerged as an important component of cellular inflammatory responses. LD lipolysis via adipose triglyceride lipase (ATGL), the enzyme that catalyses the rate-limiting step of triglyceride lipolysis, regulates inflammation in peripheral immune and non-immune cells. ATGL elicits both pro- and anti-inflammatory responses in the periphery in a cell-type dependent manner. The present study determined the impact of ATGL inhibition and microglia-specific ATGL genetic loss-of-function on acute inflammatory and behavioural responses to pro-inflammatory insult. First, we evaluated the impact of lipolysis inhibition on lipopolysaccharide (LPS)-induced expression and secretion of cytokines and phagocytosis in mouse primary microglia cultures. Lipase inhibitors (ORlistat and ATGListatin) and LPS led to LD accumulation in microglia. Pan-lipase inhibition with ORlistat alleviated LPS-induced expression of IL-1β and IL-6. Specific inhibition of ATGL had a similar action on CCL2, IL-1β and IL-6 expression in both neonatal and adult microglia cultures. CCL2 and IL-6 secretion were also reduced by ATGListatin or knockdown of ATGL. ATGListatin increased phagocytosis in neonatal cultures independently from LPS treatment. Second, targeted and untargeted lipid profiling revealed that ATGListatin reduced LPS-induced generation of pro-inflammatory prostanoids and modulated ceramide species in neonatal microglia. Finally, the role of microglial ATGL in neuroinflammation was assessed using a novel microglia-specific and inducible ATGL knockout mouse model. Loss of microglial ATGL in adult male mice dampened LPS-induced expression of IL-6 and IL-1β and microglial density. LPS-induced sickness- and anxiety-like behaviours were also reduced in male mice with loss of ATGL in microglia. Together, our results demonstrate potent anti-inflammatory effects produced by pharmacological or genetic inhibition of ATGL-mediated triglyceride lipolysis and thereby propose that supressing microglial LD lipolysis has beneficial actions in acute neuroinflammatory conditions.

* Corresponding author.
E-mail address: thierry.alquier@umontreal.ca (T. Alquier).
[1] Equal contribution

https://doi.org/10.1016/j.bbi.2024.09.027
Received 5 February 2024; Received in revised form 21 August 2024; Accepted 21 September 2024
Available online 24 September 2024

1. Introduction

Lipid droplets (LD) are dynamic organelles that have emerged as important contributors to cell metabolism and signalling. LD are principally recognised as storage sites for cholesterol esters and triglycerides (TG). The phospholipid monolayer surrounding LD contains lipases that hydrolyse TG and regulatory proteins such as perilipins (Olzmann & Carvalho, 2019). The first step of TG hydrolysis is catalysed by adipose triglyceride lipase (ATGL). ATGL hydrolyses LD-stored TG to generate diacylglyceride (DAG) and free fatty acids (Eichmann et al., 2012; Eichmann & Lass, 2015; Zechner et al., 2009). Released fatty acids serve as a cellular energy substrate or as precursors for the synthesis of lipid-mediators of inflammation such as eicosanoids (Jarc & Petan, 2020). While LD are increasingly appreciated as major players in cell metabolism and physiology (Jarc & Petan, 2020; Olzmann & Carvalho, 2019), their impact in the brain and on behaviour is much less understood.

In peripheral cells, inhibition or loss of ATGL activity promotes inflammation in a cell type-dependent manner. For example, ATGL genetic loss-of-function in white or brown adipocytes increases interleukin (IL)-6 and tumour necrosis factor (TNF)-α secretion (Kotzbeck et al., 2018; Lettieri Barbato et al., 2014a,b). Similarly, loss of ATGL in the liver enhances the expression of inflammatory markers such as macrophage chemoattractant protein 1 (CCL2), TNF-α and IL-1β in response to LPS (Jha et al., 2014). In contrast, ATGL deletion in macrophages leads to a decrease in IL-6 signalling and an increase in IL-10 and transforming growth factor (TGF)-β in response to CCL2 stimulation or in atherosclerotic mice suggesting that loss of ATGL activity promotes anti-inflammatory actions in macrophages (Aflaki et al., 2011; Lammers et al., 2011).

Recent studies have reported LD accumulation in microglia produced by inflammatory insult, disruption of lipid uptake, ageing and neurodegeneration (Khatchadourian et al., 2012; Li et al., 2023; Loving et al., 2021; Marschallinger et al., 2020; Qin et al., 2023; Li et al., 2024) suggesting microglial LD participation in neuroinflammation. The accumulation of LD in microglia in response to lipopolysaccharide (LPS) is reported to elicit the recruitment of perilipin-2 (PLIN2) and subsequent inhibition of ATGL activity (Khatchadourian et al., 2012; Wang et al., 2011). Despite these findings, the contribution of microglial ATGL to acute neuroimmune activation and associated behavioural deficits remained unknown. Here we demonstrate that pharmacological inhibition of ATGL in primary microglia or microglial ATGL loss-of-function in mice robustly reduces microglial pro-inflammatory responses to LPS and attenuates behavioural responses to LPS.

2. Methods

2.1. Animal ethics

Animal studies were conducted in accordance with guidelines of the Canadian Council on Animal Care (protocol #CM19018TAs and CM23041TAs). Adult microglia cultures were prepared in accordance with the European directive 2010/63/UE and approved by the French Ministry of Research and local ethics committees (APAFIS#: 33951). C57BL6/J mice purchased from Jackson Laboratories were used to generate pups for primary microglia. Mice were group housed on a 12 h dark-light cycle at 22–23 °C, with *ad libitum* access to standard irradiated chow diet (Teklad) and water. For studies in adult transgenic mice, age-matched littermates were used and individually housed in a reverse light cycle after genotyping. Only treatment-naive mice were used at the time of study. $ATGL^{fl/fl}$ mice were kindly donated by Dr Grant Mitchell (Wu et al., 2011) and were backcrossed at least 6 generations on the C57BL/6J genetic background (C57BL/6J, 000664). Female $ATGL^{fl/fl}$ mice on the C57BL/6J background were bred with male mice expressing tamoxifen-inducible CreERT2 recombinase and YFP under the control of the mouse CX3CR1 promoter [B6.129P2(Cg)-Cx3cr1tm2.1(cre/ERT2) Litt/WganJ, 021160], obtained from The Jackson Laboratory (Littman, 2013; Sahasrabuddhe & Singhee Ghosh, 2022). $ATGL^{+/+}$; CX3CR1-CreERT2 (CreERT2 heterozygous) controls ($CX3CR1^{ATGL}$ WT) and $ATGL^{fl/fl}$;CX3CR1-CreERT2 ($CX3CR1^{ATGL}$ KO) were obtained by breeding female $ATGL^{fl/+}$ with male $ATGL^{fl/+}$;CX3CR1-CreERT2 (CreERT2 heterozygous) to obtain littermates of all genotypes.

2.1.1. Tamoxifen delivery

Tamoxifen (Sigma) was dissolved in 10 % ethanol, 90 % corn oil by heating at 50 °C. Two doses of 10 mg tamoxifen were delivered by oral gavage at 48 h intervals. All experimental mice ($CX3CR1^{ATGL}$ WT and $CX3CR1^{ATGL}$ KO) were injected with tamoxifen. Experiments began 4 weeks post-tamoxifen to allow repopulation of non-recombined macrophages in the periphery to ensure a microglia-specific knockout (Parkhurst et al., 2013).

2.1.2. Validation of the microglial ATGL KO mouse model

Validation was performed using fluorescence activated cell sorting (FACS). Digestion, FACS and analysis were carried out as described by Legroux et al. (2015). Briefly, brains and spleens from $Cx3CR1^{ATGL}$ WT or KO male mice were digested with Collagenase D (Roche) and DNase I. Cells were recovered and separated in $CD11b^+$ microglial/macrophages or $CD11b^-$ non-microglial fractions using Percoll™ gradient followed by the pull-down cell selection method, EasyStep Mouse CD11b positive Selection Kit II (StemCell Technologies, 18970A), as per the manufacturer's instructions. Surface staining for CD45 PE-Cy7 (clone 30-F11; #552848, BD Biosciences) was carried out as previously described (Legroux et al., 2015). Cell viability was determined using Live/Dead™ (L34957, Invitrogen). The following fractions were sorted by flow cytometry: $CD45^+/YFP^+$ gated events from the $CD11b^+$ brain fraction represent microglial cells ($CD11b^+/YFP^+$); $CD45^-/YFP^-$ gated events from the $CD11b^-$ fraction represent non-microglial neural cells ($CD11b^-/YFP^-$); $CD45^+/YFP^-$ gated events from the $CD11b^+$ fraction from the spleen represent macrophages and neutrophils ($CD11b^+/YFP$). RNA was extracted from the resulting fractions with the RNeasy Plus Micro Kit (74034; Qiagen), as per manufacturer's instructions, and gene expression was quantified and characterised by qPCR as described in section 2.5.

2.1.3. Behavioural testing

Male mice were administered saline or 0.83 mg/kg LPS *i.p.* 12 h prior to behavioural testing. Behavioural testing was performed during the dark cycle. Emotionality scores were calculated as described by Guilloux et al. (2011). Briefly, z scores for each test were calculated as follows:

$$z_{observation} = \frac{Observation - meanofcontrolgroup}{Standarddeviationofcontrolgroup}$$

These $Z_{observation}$ scores were combined for the elevated plus maze (EPM) and light–dark box (LDB) tests:

$$z_{EPM} = \frac{z_{distance} + z_{time} + z_{frequency}}{numberofparameters} \text{ or } z_{LDB} = \frac{z_{time} + z_{frequency}}{numberofparameters}$$

These resulting numbers were combined into an emotionality score:

$$z_{emotionality} = \frac{z_{EPM} + z_{LDB}}{numberoftests}$$

2.1.3.1. Elevated plus maze. Testing was performed as previously reported (Sharma & Fulton, 2013). Briefly, animals were placed in the centre of the maze facing the open arm away from the experimenter. Movement was tracked using an overhead camera for 5 min. Place preference and movement were analysed using Ethovision as previously described (Sharma & Fulton, 2013).

2.1.3.2. Light-Dark box. This test was performed as we previously reported (Nakajima et al., 2023). Briefly, animals were placed in the centre of the box adjacent to the entry to the dark zone. Movement was tracked using an overhead camera for 5 min. Place preference and movement were analysed using Ethovision.

2.1.4. IBA1$^+$ cell density & soma size

After behaviour testing, animals (14 h post-*i.p.*) were euthanised with a ketamine/xylazine overdose and transcardially perfused with PBS followed by 4 % paraformaldehyde. Brains were post-fixed in 4 % paraformaldehyde for 4 h and cryopreserved in 30 % sucrose/PBS. 30 μm thick coronal sections were taken on a sliding microtome. Brain sections were stained using a free-floating method. Briefly, sections were permeabilised and blocked for 1 h at room temperature in blocking buffer (0.3 % triton-x100, 1 % normal goat serum, 50 mM glycine, PBS). Permeabilised sections were incubated overnight at 4 °C in 1:1000 rabbit anti-IBA1 (WAKO, #019–19741), followed by 1:1000 goat anti-rabbit Alexafluor 568 (Invitrogen #A-11036) for 1 h at room temperature. All antibodies were diluted in blocking buffer. A negative control was prepared without the primary antibody. Sections were mounted on glass slides with Vectashield DAPI hardset (VECTOR LABS #H1500) and imaged at 10x magnification with Zeiss Axio IMAGER M.2 for cell counting. For each brain region three sections were chosen for analysis. Regions were determined using the mouse brain atlas (Paxinos & Franklin, 2008): Cortex, motor region between bregma −0.70 mm and −1.06 mm; mediobasal hypothalamus, between bregma −1.34 mm and −1.94 mm encompassing the ventromedial and arcuate nuclei; and hippocampus, between bregma −1.58 mm and −1.94 mm. The boundary of the region of interest was marked by a dashed line and area of the region calculated (mm^2, Supplementary figure S7**G-I.**). All IBA1 + cells within the region of interest were counted on each section. Images were quantified manually using the cell counter plugin in Image J (FIJI; (Schindelin et al., 2012; Schneider et al., 2012)). The number of IBA1$^+$ cells (~100 cells per image) was then normalised to the area analysed.

Soma size of IBA1 + cells was calculated from the same images on ~ 80–120 cells/region in each experimental group. The perimeter of the soma was traced using 'polygon selections' in Image J and the 'measure' tool used to calculate soma size.

2.2. Cell culture

2.2.1. Primary neonatal mouse microglia

Primary neonatal mouse microglia were isolated from the forebrain of P1-2 mice (males and females pooled) using the method we described previously (Nakajima et al., 2023). Briefly, cerebellum, olfactory bulbs, and meninges were removed before rough homogenization with a blade. The homogenate was centrifuged at 500 g for 1 min and supernatant discarded. Homogenate was digested for 15 min in enzymatic solution (0.2 μm filter sterilised 4.5 U/mL papain [Worthington Biochemicals], glucose (5 mg/ml), cysteine (0.2 mg/ml), 1x DNAse [Worthington Biochemicals], in PBS) at 37 °C. The digest was centrifuged at 500 g for 2 min and supernatant discarded. The digest was mechanically disrupted with a serological pipette in complete media (DMEM [Gibco; 11965–092] 4.5 g/dL glucose, 10 % FBS [Gibco], 50 U/mL penicillin, 50 μg/mL streptomycin [Gibco]). Cell suspension was filtered through a 70 μm cell strainer, centrifuged at 500 g for 5 min and resuspended in complete media. Cell suspension was plated in T75 flasks (50 % forebrain/flask) and allowed to adhere for 7 days. Media was changed when astrocyte monolayer reached confluency. When microglial cells began to detach from the astrocyte layer after another 5 days in culture, microglia were dislodged by gently tapping the side of the flask and media containing microglia was centrifuged at 500 g for 10 min at RTP. Cells were counted using a hemocytometer and seeded at an appropriate density. Complete media was added to the experimental dishes and microglia were allowed to adhere for 24 h prior to the start of the experiment.

2.2.2. Primary adult mouse microglia

For adult microglia primary cultures, male C57BL/6J mice (12–15 weeks old) were euthanized by intraperitoneal pentobarbital injection (Exagon®, 300 mg/kg), 30 min post-buprenorphine administration (0.1 mg/kg, subcutaneously). Microglia isolation was performed as previously described (Herron et al., 2022). In brief, mice were transcardially perfused with ice-cold Hanks' Balanced Salt Solution (HBSS, Gibco), followed by mechanical dissociation of forebrain tissue. Single cell suspensions were prepared and centrifuged over a 37 %/70 % discontinuous Percoll gradient (GE Healthcare), mononuclear cells were isolated from the interface. Isolated adult microglia were cultured using a modified version of (Butovsky et al., 2014). Microglia were cultured for 5 days at 37 °C, 5 % CO2 in poly-D-Ornithine coated 48-well plates (9-10x10^4 cells/well in 0.5 mL) and grown in supplemented DMEM SILAC medium (Gibco), containing Glucose 2.5 mM, Lysine 0.5 mM, Arginine 0.7 mM, Glutamine 2.5 mM, mouse recombinant carrier free MCSF 10 ng/mL (R&D Systems) and human recombinant TGF-β1 50 ng/ml (Miltenyi Biotec).

2.2.3. siRNA-mediated ATGL knockdown

After plating neonatal microglia, media was removed and replaced with DMEM [Gibco; 11965–092] 4.5 g/dL glucose supplemented with 10 % FBS [Gibco], with no antibiotics. Lipofectamine RNAiMAX was used in combination with stealth siRNA (Invitrogen, #MSS227773) to achieve a knockdown of ATGL. Briefly, lipofectamine RNAiMAX and ATGL RNA or a scramble control (Invitrogen, #12935300) were diluted in OptiMEM media following manufacturer's directions to allow a final concentration of 10 nM siRNA. Preparations were added dropwise to the cultures. After 24 h, cultures were collected for validation by immunoblotting or treated with LPS as described in ***2.2.4***.

2.2.4. Cell culture treatments

For neonatal cultures, culture media was replaced 2 h prior to treatment with medium (DMEM [Winsent; 319–061-CL] containing 5 mM glucose). At time of treatment, medium was replaced with medium containing ORlistat (50 μM; MedChemExpress), ATGListatin (50 μM; MedChemExpress), etomoxir (10 μM, Caymen Chemicals) or vehicle (DMSO 0.1 % v/v) with or without LPS (0.1 μg/mL; O127:B8; Sigma). The ApoTox-Glo kit was used to measure cell viability and cytotoxicity after 6 h treatment according to manufacturer's directions (Promega, G6320). For adult microglial cultures, TGF-β1 and MCSF were removed from the medium 24 h prior to treatment. Cells were treated on Day 6 with 0.1 μg/ml LPS and ATGListatin (50 μM) or vehicle (DMSO 0.1 % v/v) for 6 h.

2.2.5. Phagocytosis

Neonatal cells were plated at 1.5 x 10^5 cells/well on 13 mm diameter glass coverslips, and treated as described in ***2.2.4***. One hour prior to the end of the treatment, 100 fluorescent beads/cell suspended in DMEM were added dropwise (Sigma, L3030). At the end of the treatment, cells were washed 3 times with PBS, and fixed with 4 % paraformaldehyde for 15 min. Cells were stained with IBA1 to ensure beads counted were internalised. Briefly, coverslips were incubated with blocking buffer for 15 min at room temperature, prior to overnight incubation in 1:500 rabbit-anti-IBA1 antibody (WAKO, #019–19741), followed by 1:1000 goat anti-rabbit Alexafluor 568 (Invitrogen #A-11036) for 1 h at room temperature. Cells were stained with Hoescht 33,342 (6 μg/mL; Invitrogen) for 5 min prior to mounting in ProLong Gold antifade mountant (Invitrogen) and allowed to set prior to imaging (20x magnification, Zeiss Axio IMAGER M.2). Internalised beads were manually counted using the counting plug-in in ImageJ (FIJI; (Schindelin et al., 2012; Schneider et al., 2012)). A minimum of 100 cells were analysed per coverslip.

2.3. Lipid droplet imaging

Primary microglia derived from pups were plated at a density of 1x10^5 on 13 mm diameter glass coverslips in 24 well plates. After 6 h treatment, cells were fixed for 15 min with 4 % paraformaldehyde at 37 °C. Intracellular LD were visualised using the neutral lipid stain BODIPY 493/503 (10 μM; DMSO; Invitrogen). Hoescht 33,342 (6 μg/mL; Invitrogen) was used to identify nuclei. After staining, cells were

mounted in ProLong Gold antifade mountant (Invitrogen) and allowed to set prior to imaging (64x oil-immersion lens; Leica SP5 multiphoton system). LD were manually counted in ImageJ, on a minimum of 100 cells/coverslip (FIJI; (Schindelin et al., 2012; Schneider et al., 2012)).

2.4. Immunoblotting

Primary mouse microglia from pups were plated at a density of $1x10^6$ in T25 flasks. After treatment, cells were lysed using modified RIPA buffer and centrifugation at 21,100 g at 4 °C for 20 min. Protein content was estimated using the Bradford method microassay procedure using a BSA standard curve (BioRad Protein Assay), as recommended by the supplier. Protein concentrations were standardised with modified RIPA buffer and lamaelli buffer. Protein separation of 10 μg sample was carried out using the BioRad mini-protean system using 12.5 % vol/vol gels and SDS-PAGE. Precision Plus Dual Colour standard (BioRad) was used to estimate protein size. Protein was transferred onto 0.2 μm nitrocellulose. Membranes were blocked 1 h with 5 % wt/vol milk in TBS and probed overnight with primary antibody (anti-ATGL: 2138S, 1:1000; anti-GAPDH: 2118S, 1:10000 [CST]). TBS-Tween 0.1 % vol/vol (TBS-T) was used to remove unbound antibody between each binding steps. Membranes were incubated with secondary antibody goat anti-rabbit conjugated to HRP (1:5000, 5 % wt/vol milk in TBS-T; #170–6515, BioRad) for 1 h. Protein was detected by incubation with SuperSignal West Pico Plus Chemiluminescence substrate (Invitrogen) for 5 min prior to imaging for 5 min with ChemiDoc Imaging system. For reblotting, membranes were stripped using Restore stripping buffer for 15 min prior to reblocking.

2.5. RNA analyses

2.5.1. Cell and tissue collection for RNA extraction

Primary mouse microglia were plated at a density of $3x10^5$ in 6 well plates and treated for 6 h prior to RNA extraction with Trizol (Invitrogen) as we described (Taïb et al., 2013). Adult microglia were treated as described in section 2.2.3 prior to extraction of total RNA using RNeasy Plus Mini Kit (Qiagen, 74106) according to the manufacturer's protocol.

$CX3CR1^{ATGL}$ WT or KO mice were administered with either a single 0.83 mg/kg or two 0.5 mg/kg injections of LPS *i.p.* (O127:B8) at 24 h intervals, or 0.9 % saline vehicle (1 mL/kg, volume matched to LPS). Animals were euthanized by decapitation under isoflurane anaesthesia 3 h after the final injection for tissue collection. Microdissections of brain regions were taken from the cortex, hippocampus and mediobasal hypothalamus (MBH) for RNA extraction. RNA was extracted from tissue samples using the Trizol method (Invitrogen) as we described (Taïb et al., 2013).

2.5.2. RNA extraction, cDNA synthesis and RT-qPCR

Extracted RNA was checked for purity and concentration using the Nanodrop 2000. For RNA extracted from neonatal microglia or tissue, cDNA was synthesised from 1 μg of RNA with M−MuLV reverse transcriptase (Invitrogen) and random hexamers as specified by the manufacturer. cDNA was diluted 1:10 prior to qPCR. qPCR master mix was composed of QuantiFast SYBR Green PCR kit (Qiagen) and forward and reverse primers (1 μM) for the relevant gene of interest. Primer sequences used are provided in Table 1. qPCR was performed for 40 cycles using the Corbett Rotor-Gene 6000 (Qiagen) and quantified using the standard curve method using Rotorgene Q series software (v2.3.1). Genes of interest were normalised to either 18S or β-actin (*in vitro*), or the geometric mean of β-actin and cyclophilin (*in vivo*) as was determined by the stability of the respective housekeeping genes. Gene expression is represented as fold change from mean of LPS-treated control groups after normalisation.

For adult microglia, 10 μL of RNA was reverse transcribed using Superscript IV VILO (Invitrogen, Life Technologies, France). cDNA was amplified using FAM-labeled Taqman® probes (Applied Biosystems/ Thermo Fisher Scientific), [ccl2 (Mm00441242_m1), il-10 (Mm01288386_m1), il-1b (Mm00434228_m1), il-6 (Mm00446190_m1), tnf-a (Mm00443258_m1), tgf-β1 (Mm01178820_m1), B2m (Mm00437762_m1) used as reference gene]. Real-time PCR reaction was performed in duplicate using a LightCycler® 480 instrument II (Roche). Data are normalized relative to B2m ($2^{(-\Delta Ct)}$).

2.6. Cytokine secretion

Primary microglia derived from pups were seeded at a density of $4x10^4$ in 96 well plates and treated for 3–24 h prior to collection of the extracellular media. CCL2 and IL-6 secretion into the extracellular media was quantified using DuoSet ELISAs (Bio-techne; DY479-05 and DY406-05 respectively), as directed by the manufacturer and normalized to cell number.

2.7. Endogenous oleate oxidation assay

Microglial cells ($1x10^6$) derived from pups were seeded in T25 flasks. Cells were incubated in phenol red free DMEM (10 mM glucose) containing 0.25 mM oleate (Sigma) pre-complexed to 0.3 % BSA and 0.1 μCi/ml [1-^{14}C] oleate (Perkin Elmer) for 24 h to label all cellular lipids

Table 1
Primers sequence.

Gene	Forward (5′-3′)	Reverse (5′-3′)
18S	TAGCCAGGTTCTGGCCAACGG	AAGGCCCCAAAAGTGGCGCA
ATGL	CTCTTGATGGCTCACATCCAA	GGCAAAGCCATCTGAGAGAC
CCL2	ATTGGGATCATCTTGCTGGT	CCTGCTGTTCACAGTTGCC
COX2	TGTCAAAACCGTGGGGAATG	GGTGGGCTTCAGCAGTAATTTG
Cyclophilin	GCTTTTCGCCGCTTGCTGCA	TGCAAACAGCTCGAAGGAGACGC
β-Actin	TTCTTGGGTATGGAATCCTGTGGCA	ACCAGACAGCACTGTGTTGGCATA
PLIN2	AGCCAACGTCCGAGATTGTT	CCTGAGACTGTGCTGGCTAC
PLIN3	TGAGAAAGGCGTCAAGACCC	TCCGCCAAAACCTTCTCAGT
IBA-1	GGATTTGCAGGGAGGAAAAG	TGGGATCATCGAGGAATTG
IL-10	CTGGCTCAGCACTGCTATGC	ACTGGGAAGTGGGTGCAGTT
IL-1β	TGCCACCTTTTGACAGTGATG	TGATGTGCTGCTGCGAGATT
IL-6	AGTCCGGAGAGGAGACTTCA	GCCATTGCACAACTCTTTTCT
iNOS	CAATGGCAACATCAGGTCGG	CGTACCGGATGAGCTGTGAA
Rac1	TACCCGCAGACAGACGTGTT	TGTCGCACTTCAGGATACCAC
TNF-α (*in vitro*)	AGGCGGTGCCTATGTCTCAG	AACTGATGAGAGGGAGGCCAT
TNF-α (*in vivo*)	GATCGGTCCCCAAAGGGATG	GCTCCTCCACTTGGTGGTTT
TGF-β1	GCTGAACCAAGGAGACGGAA	GGGCTGATCCCGTTGATTTC
HSL	GGCTCACAGTTACCATCTCACC	GAGTACCTTGCTGTCCTGTCC
ABHD5	GACCTTTTGGGTTAAGTCTA	CGTGTCATCTTCAAACATAG

including TG as described previously (Taïb et al., 2013). Prior to treatment, exogenous oleate was removed by 2 washes with PBS. Cells were then treated with β-oxidation media (phenol red free DMEM containing 1 mM carnitine, 0.3 % BSA, 2.5 mM glucose) containing vehicle, ATGListatin (50 μM) or 10 μM etomoxir and incubated for 3 h. Oxidation rate was normalized to protein content.

2.8. Targeted lipid profiling

2.8.1. Materials

Leukotriene(LT) B4, lipoxin(LX) A4, 6(S)-LXA4, 15(R)-LXA4, LXB4, maresin-1 (MaR1), protectin 1 (PD1), PDx, Resolvin D1 (RvD1), 17(R)-RvD1, RvD2, 17(R,S)-RvD4, RvD3, RvD5, RvD5n3-DPA, RvE1, 15-epi-15-F_{2t}-IsoP, 15-F_{2t}-IsoP, prostaglandin (PG)F2α, 15(R)-PGF2α, 5-*trans*-PGF2α, 8-F_{2t}-isoprostane (IsoP), 5-epi-5-F_{2t}-IsoP/5-F_{2t}-IsoP, 5(*RS*)-5-$F2_c$-IsoP, 15-F_{3t}-IsoP, 17-*trans*-PGF3α, thromboxane (TX)B2, PGD2, PGE2, 8-*iso*-PGE2, several Oxylipin MaxSpec® LC-MS Mixtures (9 eicosapentaenoic acid (EPA)-oxylipins-Mix cat#21393, 9 EPA-CYP 450 oxylipins-Mix #21394, 3 alpha-linolenic acid (ALA)/ gamma-linolenic acid (GLA) oxylipins-Mix #22638, 10 docosahexaenoic acid (DHA)-oxylipins-Mix #22280, 10 DHA-CYP 450 oxylipins-Mix #22639, linoleic acid (LA)-Mix #22638, 9 arachidonic acid (AA) oxylipins-Mix #20666) and deuterated standards: LTB4-d4, LXA4-d5, 17(*R*)-RvD1-d5, RvD2-d5, 5(*RS*)-5-F_{2c}-IsoP-d11, 5(*R*)-5-F_{2t}-IsoP-d11, 5(*S*)-5-F_{2t}-IsoP-d11, LXA4-d5, 5(S)-HETE-d8, 8-F_{2t}-IsoP-d4, 15-F_{2t}-IsoP-d4, 15-epi-15-F_{2t}-IsoP-d4, PGE2-d9, PGF2α-d4, TXB2-d4 were all obtained from Cayman Chemical (Ann Arbor, MI, USA). Butylated hydroxytoluene and indomethacin were acquired from Sigma-Aldrich (Oakville, ON, Canada). Acetonitrile (HPLC grade) and methanol (HPLC grade) were bought from Fisher Scientific (Ottawa, ON, Canada). Ammonium hydroxide and acetic acid were purchased from VWR International (Mont-Royal, QC, Canada) and ethanol 99 % from Commercial Alcohols (Toronto, ON, Canada).

2.8.2. Targeted oxylipin profiling

Neonatal microglia were seeded in T25 flasks (1x10^6 cells). After 24 h treatment (control, ATGlistatin and LPS +/- ATGListatin), cells were collected with a 1:10 methanol:water solution. 30 μL of butylated hydroxytoluene (22 M) and indomethacin (625 μM) in ethanol were added to the 750 μL collected media and cells to avoid oxidation and de novo synthesis of prostaglandins. Prior to freeze-drying, 10 μl of a 25 ng/mL mixture of deuterated standards in ethanol was added to media and cells. After the drying process, cells and media were reconstituted with 0.289 mL of 41 % ethanol in water. To ensure protein precipitation, 145 μL of acetonitrile was added to the reconstituted samples and then, allowed to rest for 5 min at −20 °C. This step was followed by centrifugation at 16,060 g for 5 min after quick specimen thawing and mixing. Supernatants were mixed to 600 μL of 0.01 M ammonium hydroxide solution in water and loaded on conditioned solid phase extraction cartridges (SPE; Oasis MAX 60 mg/3cc/30 μm). SPE cartridges were washed with ammonium hydroxide solution (0.01 M) followed with acetonitrile/methanol (8:2) solution. Oxylipins elution, drying and reconstitution was achieved as described previously (Dort et al., 2021). Samples were analysed by HPLC-MS/MS system (Bilodeau et al., 2021) with the following ternary gradient of solvents: water (A), methanol (B) and acetonitrile (C) set to 55 %, 37 % and 8 % respectively were all prepared with 0.01 % acetic acid. Solvent B was maintained for 9 min and solvent C for 2 min. Solvent C was further increased to 28.9 % at 7.5 min and maintained to this plateau until 9 min. Then, solvent B was ramped to 90 % and solvent C was decreased to 10 % over 4 min, and finally kept 2 min before returning to initial proportions for 5 min to allow column re-equilibration. Statistical analysis was achieved using Metaboanalyst 5.0 in the first instance. Oxylipins that passed the threshold of significance ($p < 0.05$, fold change (FC) expressed in log2 < 0.6 or > 1.5) were analysed further. Oxylipin levels were normalized to protein content.

2.9. Untargeted lipidomics

Primary microglia (neonatal) were seeded at 2x10^6 in 150 mm uncoated glass dishes. After 24 h treatment (control, ATGListatin, LPS +/- ATGListatin), cells were dissociated for 5 min with trypsin (0.05 %) and DNAse I. Digestion was neutralized with 10 % BSA in ice cold PBS, and cells were pelleted at 600 g for 10 min. Cells were resuspended in PBS and counted with a hemocytometer. 1.11x10^6 cells were taken for further processing and 10 % of sample taken for protein quantification. The remaining 90 % were pelleted at 600 g for 10 min, supernatant aspirated and pellet snap-frozen in liquid nitrogen and stored at −80 °C until analysis.

Lipid extraction, sample and data analysis were performed using a previously validated untargeted lipidomic workflow (Forest et al., 2018; Lefort et al., 2023; Ruiz et al., 2019). In brief, lipids were extracted from microglia pellets and spiked with six internal standards: LPC 13:0, PC19:0/19:0, PC14:0/14:0, PS12:0/12:0, PG15:0/15:0, and PE17:0/17:0 (Avanti Polar Lipids). Protein concentration was determined using BioRad Bradford dye-binding method as described in section 2.4. Samples were injected (from 1.66 to 9.92 μL according to protein concentration) into a 1290 Infinity high resolution HPLC coupled with a 6530 Accurate Mass quadrupole time-of-flight (LC-QTOF) (Agilent Technologies) via a dual electrospray ionization (ESI) source. Elution of lipids was assessed on a Zorbax Eclipse plus column (Agilent Technologies) maintained at 40 °C using a 83 min chromatographic gradient of solvent A (0.2 % formic acid and 10 mM ammonium formate in water) and B (0.2 % formic acid and 5 mM ammonium formate in methanol/acetonitrile/methyl *tert*-butyl ether [MTBE], 55:35:10 [v/v/v]). Data acquisition was performed in positive ionisation mode. All samples were processed and analyzed as a single batch. MS quality controls (QCs) were performed by (i) injecting 3 "in-house" QC samples and blanks at the beginning, middle and end of the run and (ii) monitoring the six internal standards spiked in samples for signal intensity, mass mass-to-charge ratios (m/z) and retention time (RT) accuracies. Mass spectrometry (MS) raw data processing was achieved as previously described using Mass Hunter B.06.00 (Agilent Technologies) for peak picking and an in-house bioinformatic script (Forest et al., 2018) for data processing. The resulting final dataset included 1296 high-quality MS signals, or features, defined by their m/z, RT and signal intensity and for a same unique lipid, several adducts referred as features may be annotated. Lipid annotation was achieved by MS/MS analysis for the most significant lipid features that passed the following threshold of significance (using a 2-tailed unpaired Student's t test): $p < 0.05$ and a fold change (FC) expressed in log2 < 0.8 or > 1.25 for the comparisons (i) LPS vs. DMSO, (ii) ATGLi vs. DMSO, and (iii) ATGLi + LPS vs. LPS. In addition, we used data alignment with our in-house database, which contains > 500 unique lipids with previously determined MS/MS spectra, for the remaining features. Side chains are indicated when annotated using MS/MS with certitude. When not identified, we only mentioned the total number of carbons and double bounds.

2.10. Statistics

Data is presented as mean ± S.E.M. Data prepared for analysis in Microsoft Excel and analysed and prepared for presentation using GraphPad Prism (v10.1.1). Intergroup comparisons were performed using Two-way ANOVAs with post-hoc Tukey's or Šídák's tests, One-way ANOVAs with post-hoc Tukey's or Student's t-test's as appropriate. Specific tests are detailed in figure legends. $P<0.05$ was considered significant.

3. Results

3.1. Broad inhibition of TG lipases reduces LPS-induced inflammatory responses in primary microglia

To investigate whether TG lipolysis regulates pro-inflammatory responses in microglia, the expression of cytokines was measured by qPCR in primary neonatal microglia (mixed sex cultures) treated for 6 h with LPS (0.1 μg/mL) with or without the pan-lipase inhibitor ORlistat (50 μM). Cell viability and cytotoxicity were not affected by DMSO (vehicle), ORlistat or LPS +/- ORlistat after 6 h (Supplementary Fig. S1A**&B).** In addition, DMSO (0.1 %) did not affect LPS-induced upregulation of IL-6 and CCL2 (Supplementary Fig. S1C&D). ORlistat did not affect basal expression of cytokines but attenuated LPS-induced IL-6 gene expression by 50 % ($p < 0.0001$, q = 7.952, dF=32; Fig. 1A) and IL-1β by 57 % ($p = 0.0002$, q = 6.880, dF=32; Fig. 1A). CCL2 ($p = 0.33$, q = 2.416, dF=32; Fig. 1A) and TNF-α ($p = 0.94$, q = 0.8, dF=32; Fig. 1A) expression were not affected by ORlistat compared to the LPS. Expression of the anti-inflammatory cytokine IL-10 induced by LPS was not significantly affected by ORlistat ($p = 0.10$, q = 3.339, dF=32; Fig. 1A). These findings suggest that TG lipolysis may be required for microglial upregulation of specific cytokines in response to LPS.

3.2. LPS-induced lipid droplet accumulation is associated with reduced ATGL expression in microglia

To establish whether LD accumulate in microglia exposed to LPS, as previously reported by others (Khatchadourian et al., 2012; Li et al., 2023; Loving et al., 2021; Marschallinger et al., 2020), primary neonatal mouse microglia were treated with LPS for 6 h. LPS increased accumulation of LD from a mean of 0.8 to 3.9 LD per cell ($p = 0.029$, q = 4.443, dF=9; Fig. 1B**&C**). This response was not affected by DMSO (Supplementary Fig. S1E). ORlistat induced accumulation with an average of 11.2 LD per cell ($p < 0.0001$, q = 14.92, dF=9; Fig. 1B**&C**). To determine whether LPS-induced LD accumulation could result from a decrease of TG lipolysis, the expression of the main glycerolipid lipases and proteins that regulate lipase activity were measured by qPCR. Expression of Hormone Sensitive lipase (HSL), a TG and DAG lipase, was not affected by LPS ($p = 0.2$, Fig. 1D). Co-regulators of ATGL activity, PLIN2 and ABHD5 (CGI-58) were not regulated at the transcriptional level by LPS ($p = 0.32$ & $p = 0.053$ respectively, Fig. 1D), whereas ATGL and PLIN3 were respectively downregulated by 39 % ($p < 0.0001$; Fig. 1D) and 53 % ($p < 0.0001$, Fig. 1D) in response to LPS. The downregulation of ATGL mRNA translated into reduced protein level (68 %, $p = 0.0268$, Fig. 1E-F). This suggests that LD accumulation during LPS exposure could be due to decreased ATGL expression and activity.

3.3. Pharmacological inhibition of ATGL activity dampens LPS-induced inflammatory responses in primary microglia

Since ATGL but not HSL expression was downregulated by LPS, we hypothesised that ATGL may be the main regulator of microglial LD and effector of reduced inflammation in response to pan-lipase inhibition by ORlistat. In line with results in Fig. 1B**&C**, LPS induced LD accumulation from a mean of 0.99 to 3.6 LD per cell ($p = 0.0442$, q = 3.850, dF=44, Fig. 2A**&B**) in a distinct set of experiments on primary neonatal microglia. Cell viability and cytotoxicity were not affected by inhibition of ATGL with the specific inhibitor ATGListatin (50 μM) and/or LPS after 6 h (Supplementary Fig. S1A**&B**). ATGListatin led to a similar increase in LD number to a mean of 3.8 LD per cell ($p = 0.0318$, q = 4.042, dF=44, Fig. 2A**&B**). No additive effect of LPS and ATGListatin were observed on LD number ($p = 0.6080$, q = 1.747, dF=44, Fig. 2B). To investigate whether ATGL inhibition is sufficient to recapitulate the effect of pan-lipase inhibition (Fig. 1A), primary neonatal microglial cultures were treated for 6 h with ATGListatin and/or LPS. In neonatal cultures, inhibition of ATGL decreased LPS-induced IL-6 (46 %, $p < 0.0001$; Fig. 2C), CCL2 (35 %, $p = 0.0051$; Fig. 2C) and IL-1β (38 %, $p < 0.0001$; Fig. 2C) expression. In primary adult microglial cultures (from male mice), ATGL inhibition recapitulated the majority of the effects observed in neonatal cultures, with ATGListatin treatment decreasing IL-6, CCL2 and IL-1β by 44 % ($p = 0.003$), 44 % ($p = 0.0189$) and 38 % ($p = 0.0026$) respectively in LPS-treated conditions (Supplementary Fig. S1F). ATGL inhibition also enhanced the LPS-induced expression of the anti-inflammatory cytokine IL-10 by 55 % in neonatal cultures ($p = 0.0097$; Fig. 2C). Conversely, LPS-induced expression of TGF-β was downregulated 33 % by ATGListatin ($p = 0.0123$; Fig. 2C). These effects were not recapitulated in adult microglia cultures, in which ATGListatin induced a 50 % decrease in IL-10 expression ($p = 0.0241$; Supplementary Fig. S1F) and did not affect TGF-β expression. ATGL inhibition did not affect LPS-induced expression of TNF-α in neonatal ($p = 0.3$ Fig. 2C) and adult cultures ($p = 0.4$, Supplementary Fig. S1F) suggesting that ATGL specifically regulates a subset of pro-inflammatory cytokines.

Importantly, these changes led to a decrease in LPS-induced cytokine secretion in neonatal microglia, mostly observed 12–24 h post-treatment (Fig. 2D**&E**). IL-6 secretion was decreased by 67 % and 69 % respectively (12 h: $p = 0.011$, q = 2.13, dF=152; 24 h: $p < 0.0001$, q = 5.878, dF=152; Fig. 2D), while CCL2 secretion was decreased at 12 h (62 %, $p < 0.0001$, q = 8.044, dF=204; Fig. 2E) and 24 h (48 %, $p < 0.0001$, q = 7.935, dF=204; Fig. 2E) in ATGListatin + LPS vs. LPS conditions. LPS-induced TNF-α secretion was not altered by ATGListatin at either 12 h ($p = 0.5$, Supplementary Fig. S1G) or 24 h ($p = 0.8$, Supplementary Fig. S1H). These data suggest that inhibition of ATGL activity recapitulated in most part the effect of ORlistat and was sufficient to reduce LPS-induced pro-inflammatory responses. Importantly, the effect of ATGL inhibition on IL-6 and CCL2 secretion was recapitulated with siRNA-mediated knock-down of ATGL validated by western blot (Supplementary Fig. S1I) in neonatal microglia. LPS-induced IL-6 secretion was decreased by 44 % ($p = 0.0021$, t = 4.293, dF=12; Fig. 2F) and LPS-induced CCL2 secretion reduced by 36 % after 24 h ($p = 0.0182$, t = 2.965, dF=16; Fig. 2G) in cells with ATGL knock-down.

To assess whether the effects of ATGL inhibition on LPS-induced cytokines are related to changes in reactive oxygen and nitrogen species, we measured expression of iNOS, Rac1 (a major regulator of NADPH oxidase), and COX2. COX2 expression is known to be upregulated by LPS-induced reactive oxygen species (Wang et al., 2004). While LPS increased iNOS and COX2 expression, ATGL inhibition did not affect these responses (Supplementary Fig. S1J). Rac1 expression remained stable across the different conditions. These data suggest that the effect of ATGListatin is not associated to changes in the expression of key pro-inflammatory markers involved in oxidative/nitrative stress.

ATGL activity releases fatty acids which can be used as substrate for fatty acid oxidation (FAO) in the mitochondria. To assess whether the action of ATGListatin on LPS responses could be dependent on reduced FAO, we measured the effect of ATGListatin on FAO and tested whether etomoxir-induced FAO inhibition recapitulates the effect of ATGL inhibition on cytokine expression in neonatal microglia. ATGListatin and etomoxir reduced FAO by 27 % ($p = 0.0306$, q = 3.953, dF=18, Supplementary Fig. S2A) and 46 % ($p < 0.0001$, q = 8.555, dF=18, Supplementary Fig. S2A), respectively. Despite a slight reduction of IL-6 expression, etomoxir did not recapitulate the effect of ATGListatin on IL-1β and CCL2 expression nor CCL2 and IL-6 secretion in response to LPS (Supplementary Fig. S2B-D).

3.4. ATGL inhibition promotes phagocytosis

Accumulation of LD in microglia in neurodegenerative states has been associated with impaired phagocytosis (Li et al., 2024). We assessed whether acute LD accumulation induced by ATGListatin and/or LPS modulates phagocytosis in neonatal microglia. Inhibition of ATGL with ATGListatin (6 h) in control conditions significantly increased both the percentage of phagocytotic cells (145 %, $p = 0.0404$, Fig. 3A**&B**) and number of fluorescent beads/cell in neonatal cultures (29 %, $p = 0.0475$,

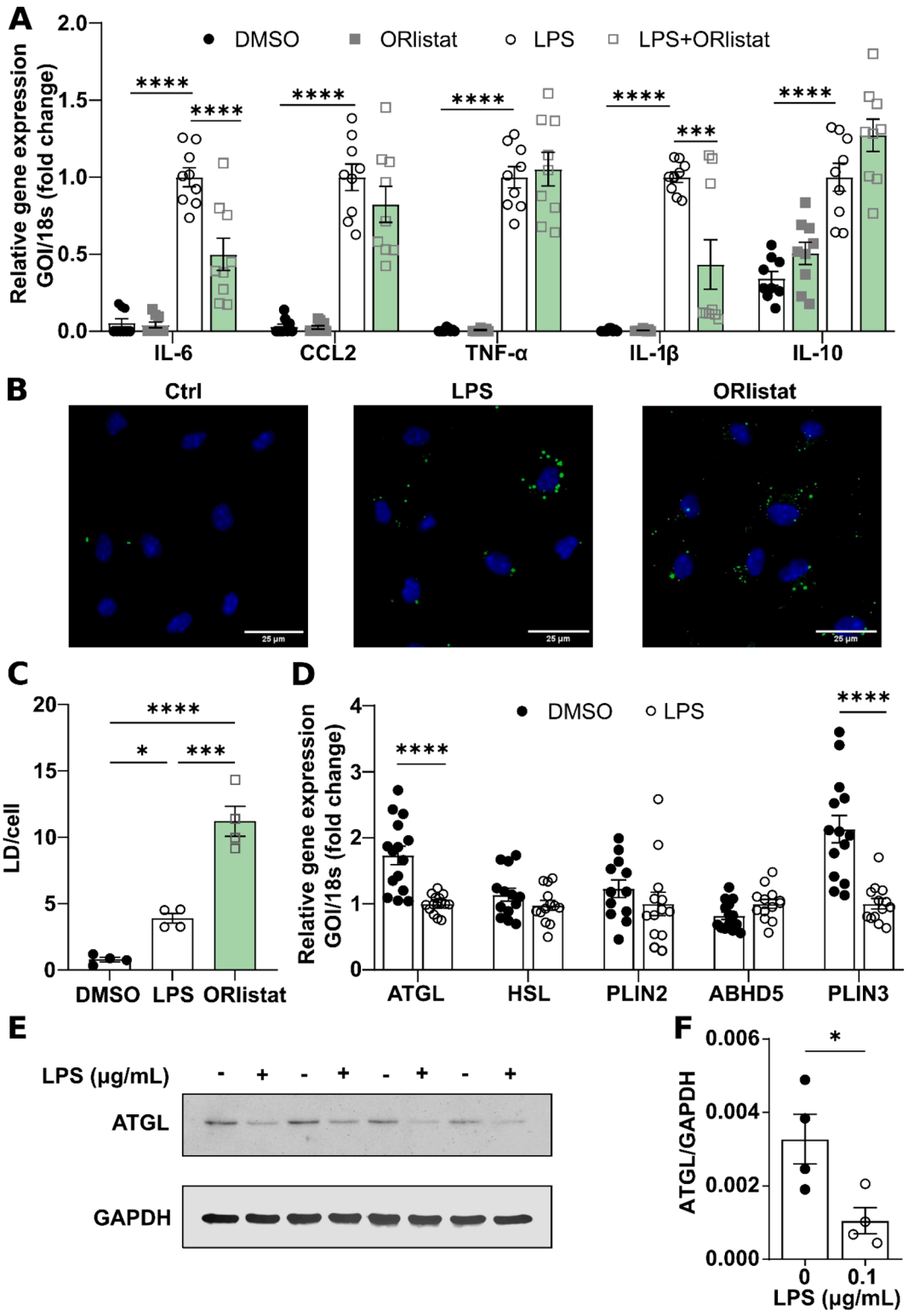

Fig. 1. Lipolysis inhibition by ORlistat reduces LPS-induced inflammatory responses in primary microglia. **A.** Relative gene expression of cytokines after 6 h with 0.1 µg/mL LPS±50 µM ORlistat (n = 9). Two-way ANOVA with post-hoc Tukey. **B.** Representative images of primary neonatal microglia treated 6 h with LPS or ORlistat and stained with BODIPY (green) and Hoescht (blue). 25 µm scale. **C.** Average number of lipid droplets (LD) per cell (n = 4, 3–4 fields of view/n). One-way ANOVA with post-hoc Tukey **D.** Relative gene expression of lipases and co-regulators (n = 12–15). **E.** Representative immunoblot and **F.** densitometric analysis of ATGL protein level relative to GAPDH expression (n = 4). Student's *t*-test. * $p < 0.05$; ** $p < 0.01$; *** $p < 0.001$; **** $p < 0.0001$. (For interpretation of the references to colour in this figure legend, the reader is referred to the web version of this article.)

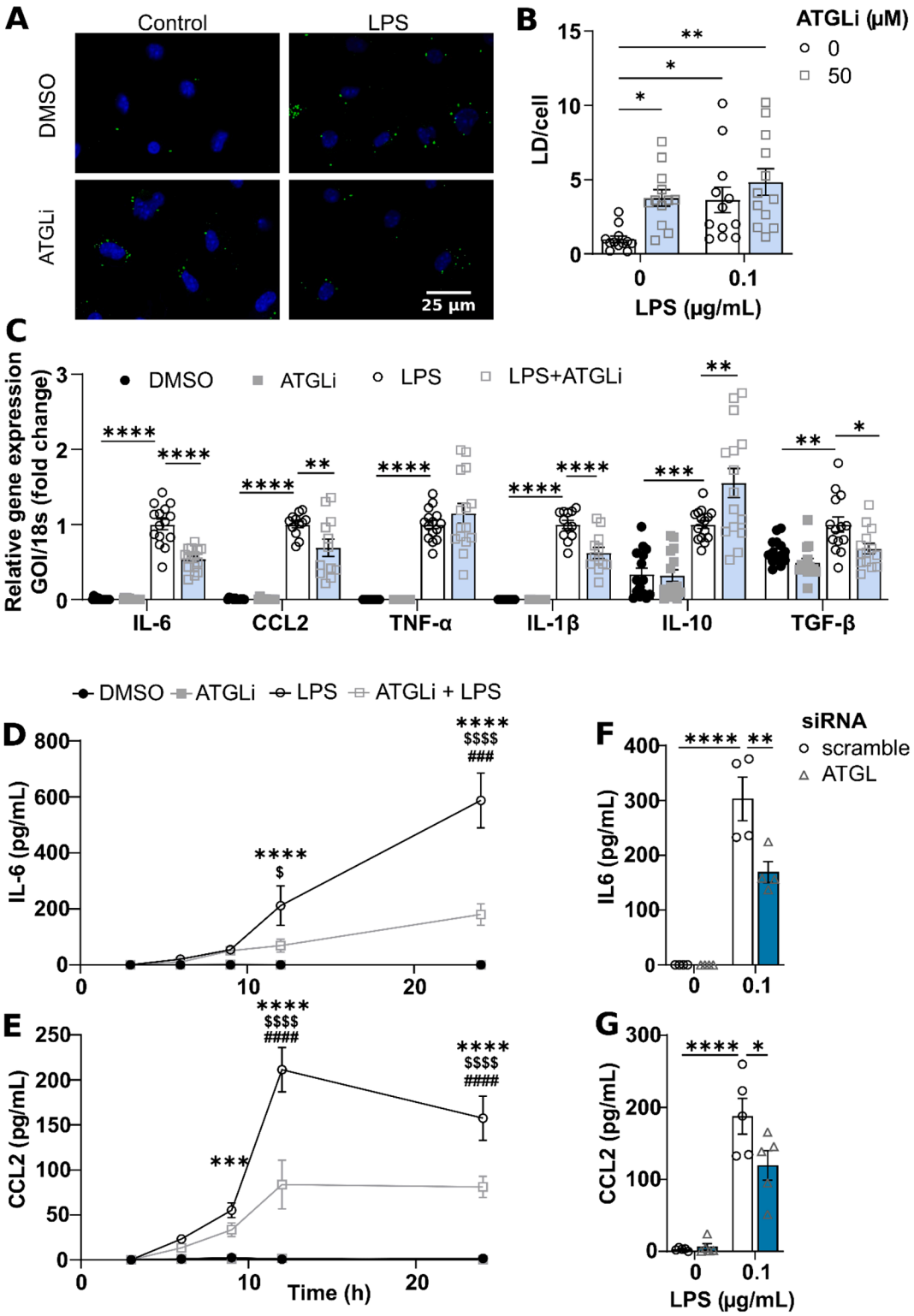

Fig. 2. ATGL inhibition reduces LPS-induced inflammatory responses in primary microglia. Effect of treatment with 0.1 µg/mL LPS±50 µM ATGListatin on LD and cytokines. **A.** Representative images of primary neonatal microglia treated 6 h with LPS or ATGListatin and stained with BODIPY (green) and Hoescht (blue). 25 µm scale. **B.** Average number of lipid droplets (LD) per cell (n = 4, 3 fields of view/n). Two-way ANOVA with post-hoc Tukey. **C.** Relative gene expression of cytokines in neonatal microglia (n = 15). Extracellular cytokine concentration of **D.** IL6 and **E.** CCL2 from neonatal microglia up to 24 h after treatment. n = 10–15; (* LPS vs ctrl; # LPS vs ATGListatin + LPS; $ ATGLi vs ATGLi + LPS). Two-way ANOVA with post-hoc Tukey. Extracellular cytokine concentration of **F.** IL6 and **G.** CCL2 from neonatal microglia after siRNA-mediated knockdown of ATGL 24 h after LPS treatment. Two-way ANOVA with post-hoc Šídák. * $p < 0.05$; ** $p < 0.01$; *** $p < 0.001$; **** $p < 0.0001$. (For interpretation of the references to colour in this figure legend, the reader is referred to the web version of this article.)

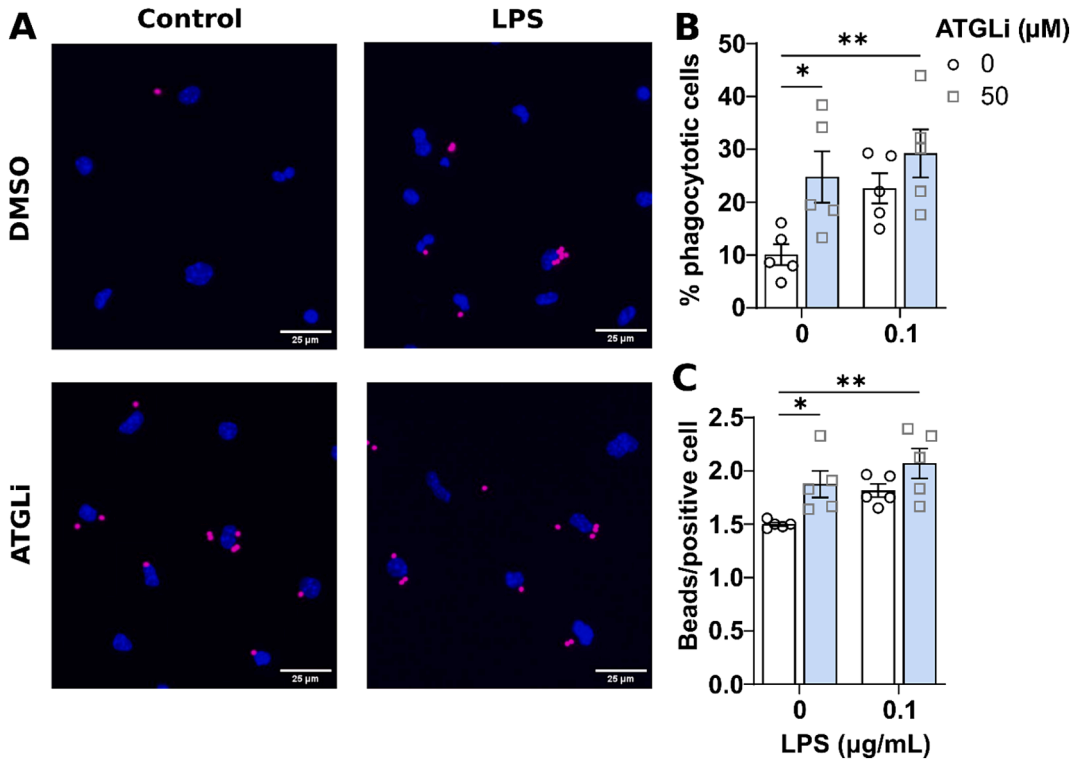

Fig. 3. Inhibition of ATGL increases microglial phagocytosis. Effect of 6 h treatment with 0.1 µg/mL LPS±50 µM ATGListatin on phagocytosis in neonatal microglia. **A.** Representative images of phagocytosed fluorescent beads (magenta) and nuclei (blue). 25 µm scale. **B.** Percentage of cells containing beads. **C.** Average number of beads per phagocytotic cell. N=5 (with ~ 100 cells counted/coverslip), Two-way ANOVA with post-hoc Šídák. * $p < 0.05$; ** $p < 0.01$. (For interpretation of the references to colour in this figure legend, the reader is referred to the web version of this article.)

Fig. 3A-C). While LPS led to a non-significant trend towards increased phagocytotic cells (124 %, $p = 0.09$, Fig. 3B) and beads/cell (21 %, $p = 0.11$, Fig. 3C), both parameters were significantly increased by 6 h LPS and ATGL inhibition (189 %, $p = 0.0071$; 38 %, $p = 0.0026$ respectively; Fig. 3B**&**C).

3.5. Inhibition of ATGL reduces LPS-induced prostanoid release

Oxylipins are lipid mediators of inflammation that can be produced by polyunsaturated fatty acids derived from TG lipolysis. We investigated the impact of ATGL inhibition on intracellular and extracellular levels of oxylipins in neonatal microglia treated for 24 h with ATGListatin and/or LPS. Among 88 oxylipin species analysed by targeted LC-MS/MS, 79 had detectable levels. The overall changes in extracellular and intracellular oxylipins are shown as heatmaps in Supplementary Fig. S3. Using principal component analysis (PCA) no samples were identified as outliers. A partial separation between the LPS condition and all other conditions was observed in the culture media (Fig. 4A). Partial separation was also observed between the vehicle and ATGListatin conditions, suggesting that inhibition of ATGL altered the release of oxylipin species at baseline. 95 % of the variance between groups was explained by component 1, and 4.1 % of the remaining variance was explained by component 2. For intracellular oxylipins, no separation between groups was observed using PCA (Fig. 4D). Volcano plot analysis was performed to identify oxylipin species significantly affected by LPS vs. controls (Fig. 4B, E), and by ATGListatin + LPS compared to LPS (Fig. 4C, F). FC>1.5 and < 0.6 and $p < 0.05$ was used as the threshold to identify significant changes in oxylipin levels. Three prostanoids (arachidonic acid metabolites) were significantly increased by LPS and reduced by co-treatment with ATGListatin in the media: prostaglandin E2 (PGE_2), D2 (PGD_2), and thromboxane B2 (TXB_2). PGF_{2a} level in the intracellular fraction was regulated in a similar manner (ctrl vs. LPS, Fig. 4E**;** LPS vs. ATGListatin + LPS, Fig. 4F). Of note, co-treatment with ATGListatin also reduced levels of oxidative stress markers in the media including 4 isoprostanes namely 5(*RS*)-5-F_{2c}-IsoP, 15-epi-15-F_{2t}-IsoP, 5-epi-5-F_{2t}-IsoP and 15(*R*)-PGF2α (Fig. 4C). Two-way ANOVA analysis revealed that inhibition of ATGL decreased LPS-induced PGE_2 release by 81 % ($p < 0.0001$, q = 8.482, dF=20, Fig. 5A), PGD_2 by 82 % ($p = 0.0002$, q = 7.441, dF=20, Fig. 5A), and TXB_2 by 71 % ($p = 0.0003$, q = 7.118, dF=20, Fig. 5A). The intracellular level of PGF_{2a} was reduced by 51 % ($p = 0.0023$, q = 5.940, dF=20, Fig. 5B).

3.6. ATGL inhibition alters ceramide species in neonatal microglia

Lipid-derived molecules are important to many aspects of the inflammatory response beyond production of cytokines and prostanoids. To assess more broadly the impact of ATGL activity on the microglial lipidome, untargeted lipidomic profiling was performed by LC-MS/MS on primary cells treated for 24 h with LPS and/or ATGListatin. Considering $p < 0.05$ and FC>1.25 and < 0.8 as significant for the annotated MS signals, we found 4 lipids significantly affected by LPS vs. DMSO conditions (Fig. 6A), and 5 lipids regulated by ATGListatin vs. DMSO (Fig. 6B). Two identified lipids were significantly altered by ATGListatin vs. LPS (Fig. 6C). Cer(d18:0/24:0) was significantly upregulated ($p = 0.028$, FC=2.52) whereas Cer(d40:1) was significantly downregulated ($p = 0.03722$, FC=0.50). Four lipids were modulated by ATGListatin + LPS vs. LPS conditions (Fig. 6D). These lipids were predominantly dihydroceramides and ceramides. Three dihydroceramide species were significantly upregulated by LPS: Cer(d18:0/16:0), $p = 0.0186$, FC=2; Cer(d40:0), $p = 0.0454$, FC=1.81; and Cer(d18:0/24:0), $p = 0.0111$, FC=1.72 (Table 2). Co-treatment with ATGListatin appeared to exacerbate the effect of LPS, further upregulating most of the identified ceramide species in the same direction as LPS treatment alone. A similar pattern was observed for sphingomyelin (d18:0/18:0) which was increased by ATGListatin + LPS. However, Cer(d18:1/24:0) ($p = 0.0156$, FC=0.56) and Cer(d40:1) ($p = 0.0289$, FC=0.56) were

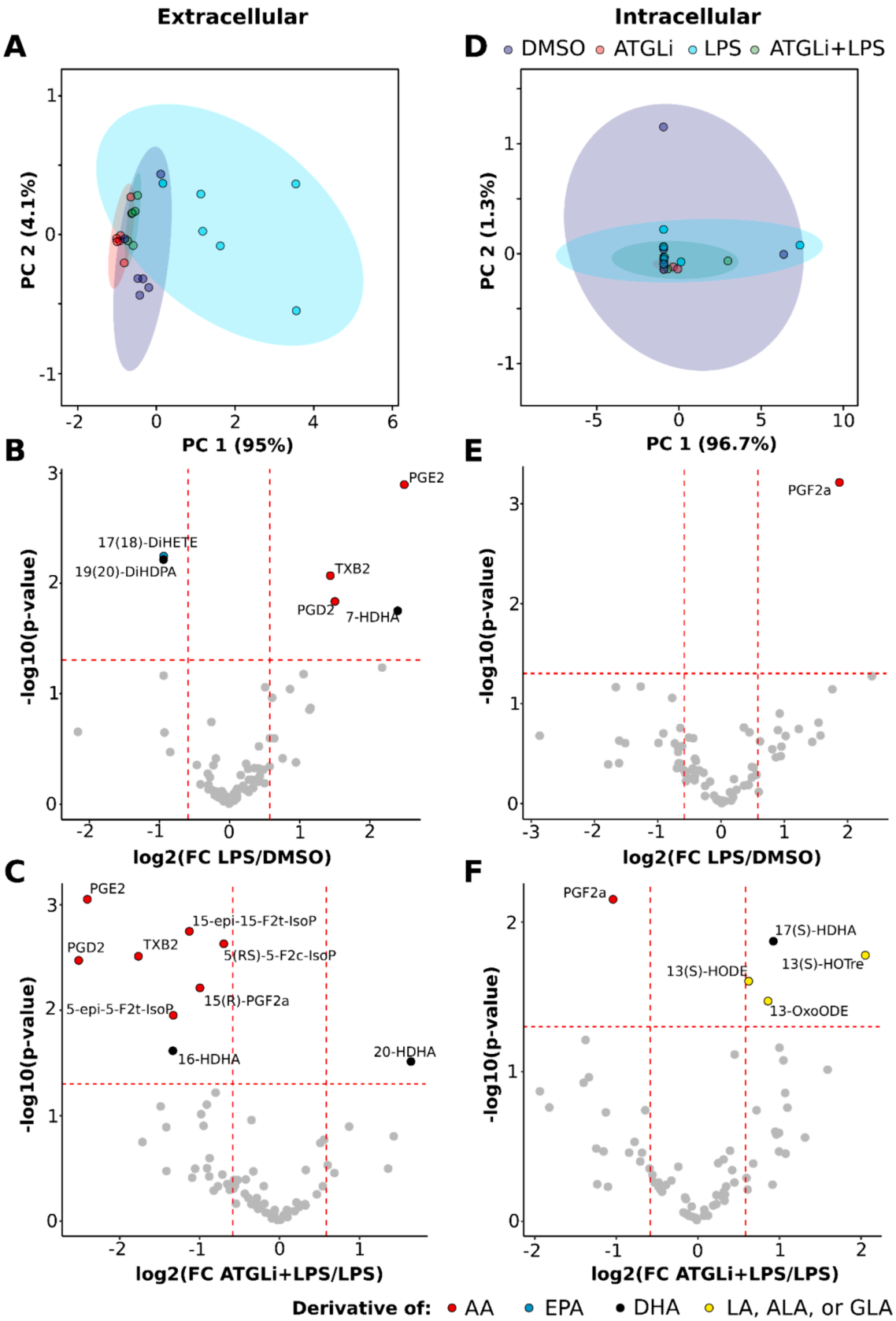

Fig. 4. Inhibition of ATGL alters the release of oxylipins. Targeted oxylipin profiling by LC-MS/MS in response to 24 h treatment with 0.1 mg/mL LPS±50 μM ATGListatin in neonatal microglia cultures (n = 6). PCA analysis of **A.** extracellular and **D.** intracellular oxylipins. Volcano plot comparing LPS vs. vehicle in the **B.** extracellular and **E.** intracellular fraction. Volcano plot comparing ATGListatin + LPS vs. LPS in the **C.** extracellular and **F.** intracellular fraction. FC=1.5, $p < 0.05$.

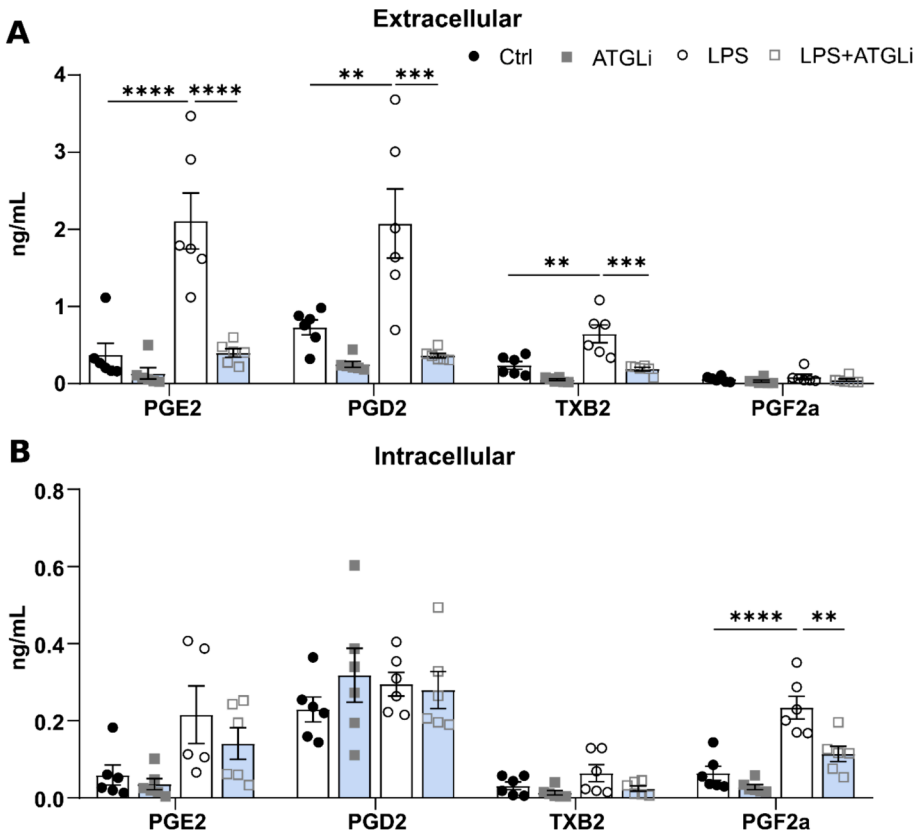

Fig. 5. Inhibition of ATGL alters LPS-induced prostanoid release. Effect of 24 h treatment with 0.1 mg/mL LPS±50 μM ATGListatin on oxylipins identified by LC-MS/MS in neonatal microglia cultures. Altered oxylipins in the **A.** extracellular and **B.** intracellular fractions (n = 6). Two-way ANOVA with post-hoc Tukey. ** $p < 0.01$; *** $p < 0.001$; **** $p < 0.0001$.

significantly downregulated by co-treatment with ATGListatin + LPS vs. LPS, whereas LPS non-significantly increased these species (Table 2). The overall changes (significant and non-significant) in identified ceramides, sphingomyelins and TG are shown as heatmaps in Supplementary Fig. S4.

3.7. *Microglia specific ATGL loss-of-function reduces LPS-induced inflammation and sickness-like behaviour*

To determine the impact of ATGL on the microglial inflammatory response *in vivo* we generated a novel mouse model with specific and inducible knock out of ATGL in microglia in adult mice (CX3CR1^{ATGL} WT and KO, see methods). To validate loss of ATGL specifically in microglia, FACS was performed 4 weeks after tamoxifen administration in adult male mice. Relative expression of IBA1 and ATGL was measured by qPCR in YFP$^+$/CD11b$^+$ (microglial/macrophage) and YFP$^-$/CD11b$^-$ (non-microglial) cell populations from brain and spleen samples (Supplementary Fig. S5A-D). As expected, IBA1 was expressed in the YFP$^+$/CD11b$^+$ population and undetectable in the YFP$^-$ cells. IBA1 expression was not affected in CX3CR1^{ATGL} KO YFP$^+$/CD11b$^+$ brain cells ($p = 0.31$). In YFP$^+$ cells, ATGL expression was decreased by 95 % ($p = 0.017$) in CX3CR1^{ATGL} KO mice compared to control Cx3CR1-CreER-YFP littermates (CX3CR1^{ATGL} WT). ATGL expression was not affected in YFP$^-$ brain cells (Supplementary Fig. S5B) and CD11b + spleen cells (Supplementary Fig. S5D) thereby confirming that loss of ATGL expression was restricted to microglia. Loss of microglial ATGL did not affect the gross phenotype of adult male mice, including body weight or anxiety-like behaviour in basal conditions measured by elevated plus maze (EPM) and open field (OF) tests (Supplementary Fig. S5**E-J**).

To assess whether loss of ATGL in microglia affects pro-inflammatory responses induced by LPS, male mice received an LPS injection (*i.p.*, 0.83 mg/kg) and expression of cytokines was measured in brain regions implicated in sickness- and anxiety-like behaviours (cortex and hippocampus) (Capuron & Miller, 2011; Ghasemi et al., 2022) as well as in neuroendocrine and autonomic responses (hypothalamus) induced by LPS (Becskei et al., 2008; Soto-Tinoco et al., 2016). We focused our analyses on pro-inflammatory cytokines known to be induced by LPS and to have a causal role in LPS-induced sickness- and anxio-depressive behaviours notably IL-6, IL-1β and TNF-α (Brymer et al., 2019; Capuron & Miller, 2011; Song et al., 2020; Ting et al., 2020). Cytokines expression was measured 3 h after LPS administration (Fig. 7A-C, Supplementary Fig. S6A) as described previously (Demers et al., 2020). As expected, LPS increased the expression of IL-6, CCL2, TNF-α and IL-1β in all regions analysed including the cortex, hippocampus and mediobasal hypothalamus (MBH) of male CX3CR1^{ATGL} WT mice (Fig. 7A-C). Consistent with our *in vitro* observation, loss of microglial ATGL expression decreased LPS-induced IL-1β expression in the MBH (40 %, $p = 0.0144$, Fig. 7A) and cortex (45 %, $p = 0.009$, Fig. 7B) along with IL-6 in the MBH (57 %, $p = 0.0032$; Fig. 7A). Although not statistically significant, there was a trend towards reduced LPS-induced IL-1β, IL-6, CCL2 and TNF-α in the other brain regions of CX3CR1^{ATGL} KO male mice (Fig. 7A-C). A similar decrease of LPS-induced IL-6 expression was observed in CX3CR1^{ATGL} KO mice injected with 2 lower doses of LPS (*i.p.*, 0.5 mg/kg, Supplementary Fig. S6B) in the MBH (53 %, $p = 0.0035$) and cortex (52 %, $p = 0.0005$) but not in the hippocampus ($p = 0.25$, Supplementary Fig. S6D-F). To assess whether loss of ATGL altered the number of microglial cells, we measured the density of IBA1 + cells in the same brain regions of animals injected with a single dose of LPS (Supplementary Fig. S6C & 6G-**I**). In the MBH and cortex, LPS increased the density of microglia in CX3CR1^{ATGL} WT mice by 83 % ($p = 0.0016$) and 48 % ($p = 0.0279$) respectively 14 h after a single dose of LPS (0.83

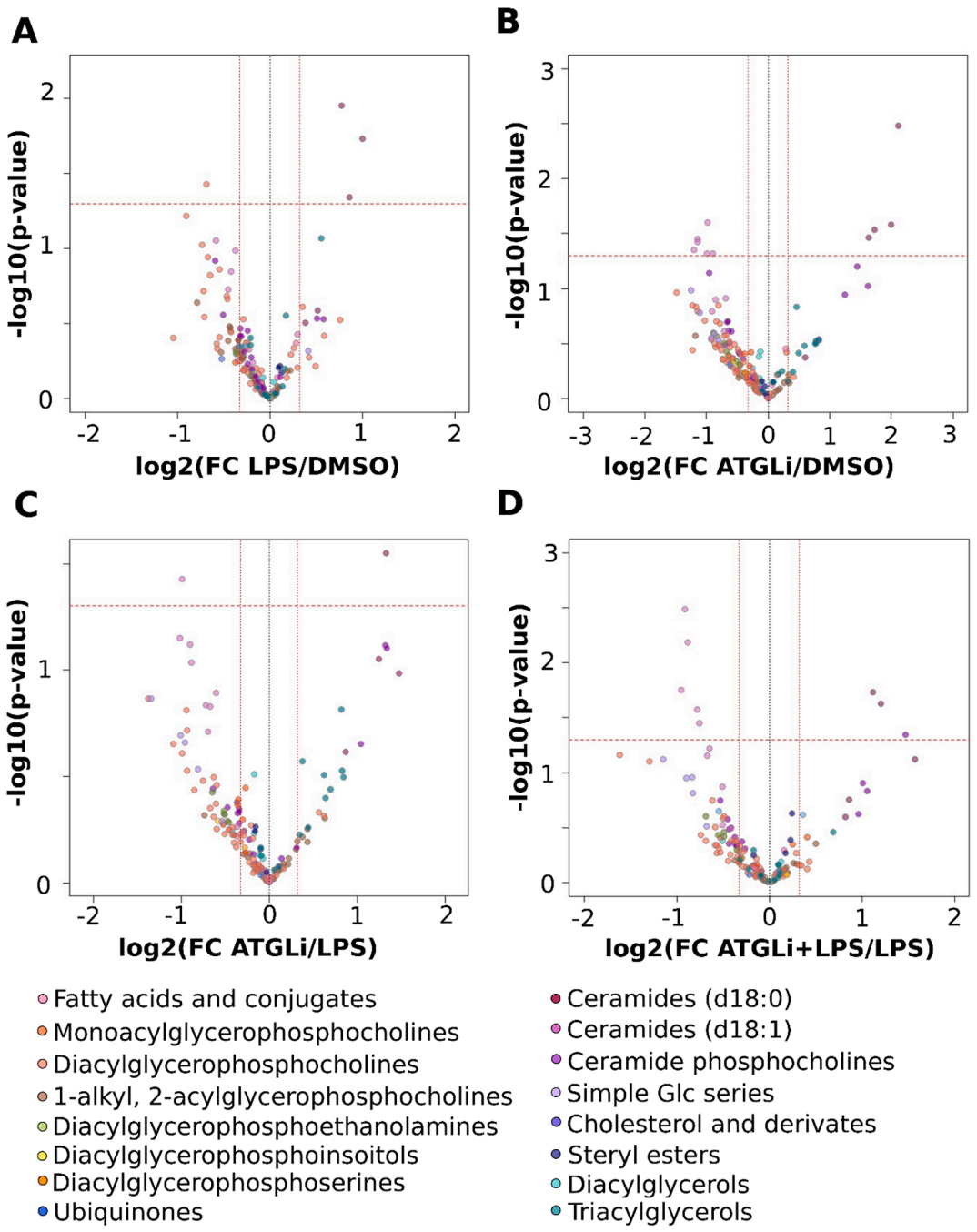

Fig. 6. Inhibition of ATGL alters microglial ceramide profile. Effect of 24 h treatment with 0.1 mg/mL LPS±50 μM ATGListatin on the lipidome identified by LC-MS/MS in neonatal microglia cultures (n = 6). Volcano plots showing 162 MS signals or lipid features (154 unique lipids), represented by a dot and defined by RT, *m/z* and signal intensity, annotated either by alignment with our in-house database to specific lipid entities (145 features; 142 unique lipids) or by MS/MS (17 features; 12 unique lipids). Coloured dots referring to the various lipid subclasses are indicated in the legend. Features were defined as significantly different with a $p < 0.05$, FC>1.25. **A.** LPS vs. DMSO, **B.** ATGListatin vs. DMSO, **C.** ATGListatin vs. LPS and **D**. ATGListatin and LPS vs. LPS.

mg/kg *i.p*) (Fig. 7D, E**, G, H**). This increase in IBA1 + cells was not observed in CX3CR1^{ATGL} KO mice injected with LPS (MBH, 51 % decrease vs. WT LPS, $p = 0.0001$, Fig. 7D**&G**; cortex, 32 % decrease vs. WT LPS, $p = 0.0176$, Fig. 7E**&H**). Microglia density was not affected in the hippocampus across the experimental groups (Fig. 7F**&I**). Microglial morphology is known to be associated with microglial activity, with an enlargement of soma size induced by pro-inflammatory stimulus (Savage et al., 2019). We observed a 52 % increase in soma size of IBA1^{+} cells in the MBH of LPS-injected WT mice (Supplementary Fig. S6J, $p <$ 0.0001), a response that was mitigated by loss of microglial ATGL ($p <$ 0.0001). Soma size was not affected by LPS or loss of ATGL in other brain regions (Supplementary Fig. S6K**-L**).

Neuroinflammation is well known to contribute to psychomotor and emotional disturbances induced by systemic infection. To establish whether microglial ATGL affects sickness- and anxiety-like behaviours induced by LPS, mice were injected with saline or LPS (*i.p.*, 0.83 mg/kg) and were subjected to EPM and light–dark box (LDB) tests 12 h after the injection. In agreement with EPM results presented in Supplementary Fig. S5E**-G** in naïve mice (no injection), distance, entries and time in open arms were similar in CX3CR1^{ATGL} WT and KO male mice treated with saline. In CX3CR1^{ATGL} WT mice, LPS reduced locomotor activity by 28 % during the EPM compared to control littermates injected with

Table 2
Significantly altered ceramides and sphingomyelin.

Annotated ID	LPS vs Ctrl			ATGLi vs Ctrl			ATGLi + LPS vs LPS		
	p	FC (abs)		p	FC (abs)		p	FC (abs)	
Cer(d18:0/16:0) [M+H]+	**0.0186**	2.00	up	0.4183	1.52	up	0.1317	1.82	up
Cer(d18:0/24:0) [M+H]+	**0.0111**	1.72	up	**0.0033**	4.33	up	**0.0124**	2.17	up
Cer(d18:0/24:1) [M+H]+	0.2577	1.43	up	**0.0262**	3.99	up	**0.0422**	2.98	up
Cer(d40:0) [M+H]+	**0.0454**	1.81	up	**0.0290**	3.31	up	0.1987	1.77	up
Cer(d18:1/24:0) [M+H]+	0.1033	0.77	down	**0.0252**	0.51	down	**0.0033**	0.53	down
Cer(d18:1/24:1) [M+H]+	0.7734	0.94	down	**0.0482**	0.50	down	0.0700	0.63	down
Cer(d40:1) [M+H-H2O]+	0.8959	1.03	up	0.1264	0.56	down	**0.0289**	0.58	down
Cer(d41:1) [M+H]+	0.4512	0.79	down	0.2453	0.61	down	0.2988	0.70	down
Cer(d42:2) [M+H-H2O]+	0.0879	0.67	down	0.1605	0.53	down	0.3206	0.75	down
SM(d18:0/18:0) [M+H]+	0.2939	1.50	up	0.0946	3.08	up	**0.0448**	2.78	up

Table 2 Ceramides and sphingomyelin altered by LPS and/or ATGListatin Effect of LPS (0.1 μg/mL) ± ATGListatin (50 μM) during 24 h on microglial ceramides (Cer) and sphingomyelin (SM) identified by untargeted LC-MS/MS in neonatal microglia. Data are represented as absolute (abs) fold change (FC), with column indicating upregulation or downregulation. $p < 0.05$, FC>1.25 considered as significant upregulation (red) or downregulation (blue).

saline ($p = 0.0058$, t = 3.363, dF=34, Fig. 8A). LPS-induced hypo-locomotion was abrogated in CX3CR1^{ATGL} KO animals (32 % increase, $p = 0.0349$, t = 2.662, dF=3, Fig. 8A). Time and number of entries in the open arms were not affected by LPS (Fig. 8B**&C**) in agreement with our previous study (Demers et al., 2020). During the LDB test, distance was reduced in saline-treated CX3CR1^{ATGL} KO male mice vs. control littermates. While LPS led to hypo-locomotion in control littermates (48 %, $p = 0.0015$, t = 4.115, dF=28, Fig. 8D) as well as reduced time (47 %, $p = 0.0135$, t = 3.201, dF=28, Fig. 8E) and number of entries (54 %, $p = 0.0052$, t = 3.571, dF=28, Fig. 8F) in the light zone compared to saline controls, these responses were absent in CX3CR1^{ATGL} KO male mice after LPS *i.p.* when compared to CX3CR1^{ATGL} KO saline controls ($p = 0.9993$, t = 0.3003, dF=28, Fig. 8D; $p > 0.99$, t = 0.06004, dF=28, Fig. 8E; $p = 0.2031$, t = 2.001, dF=28, Fig. 8F). When the data from both tests were combined into a measure of emotionality (z-score) as described by Guilloux et al. (2011), we found that LPS strongly reduced the z-score ($p = 0.0002$, t = 4.862, dF=27, Fig. 8G) in control littermates while it was not affected in CX3CR1^{ATGL} KO mice compared to CX3CR1^{ATGL} KO saline controls ($p = 0.3219$, t = 1.744, dF=27, Fig. 8G). This suggests that ATGL-dependent LD lipolysis is implicated in LPS-induced mood disorders.

4. Discussion

LD dynamics and associated TG metabolism contribute to immune cell function and response to inflammatory insults. The present study significantly extends our understanding of LD function in immunity with evidence suggesting that microglial LD lipolysis participates in neuro-immune activation and associated behavioral responses. Microglial ATGL is demonstrated to regulate basal LD lipolysis and phagocytosis in addition to reducing the expression and secretion of pro-inflammatory cytokines in response to LPS. Consistent with these findings, microglial-specific genetic deletion of ATGL attenuated microglia density and pro-inflammatory cytokine responses to LPS as well as consequent anxiety- and sickness-like behaviours. These results may be explained by reduced release of pro-inflammatory prostanoids and altered balance between dihydroceramides and ceramides in microglia elicited by ATGL inhibition. Collectively, our results suggest that blockage of ATGL-dependent LD lipolysis in microglia mitigates acute neuroimmune and behavioural responses to LPS by reducing the generation of fatty acid-derived mediators of inflammation.

Consistent with previous findings in primary microglia (Li et al., 2023; Marschallinger et al., 2020) or microglial cell lines (Khatchadourian et al., 2012), LPS treatment led to LD accumulation, similar in magnitude to inhibition of ATGL. LPS induced a robust decrease of ATGL mRNA and protein levels, without affecting HSL expression. This suggests LPS-induced LD accumulation stems from decreased ATGL-dependent lipolysis. In line with this, we found that ATGL inhibition was sufficient to increase LD number in unstimulated conditions suggesting persistent lipolytic activity in microglia. Khatchadourian *et al.* attributed LPS-induced LD accumulation to increased expression of ATGL regulatory protein PLIN2 (Khatchadourian et al., 2012). Although PLIN2 mRNA level was not affected by LPS in our study, PLIN3 expression was strongly reduced by LPS which may contribute to decreased lipolysis (Itabe et al., 2017). LPS-induced downregulation of ATGL and anti-lipolytic action promoting LD accumulation in microglia are consistent with previous studies in macrophages (Feingold et al., 2012; Huang et al., 2014). Together, these data suggest that LPS promotes microglial LD accumulation by reducing ATGL-dependent lipolysis. Additional work will be needed to identify the signalling and molecular pathway(s) by which LPS downregulates ATGL expression.

Experiments using the TG lipase ORlistat or the specific inhibitor of ATGL (ATGListatin) reliably demonstrated that TG lipase inhibition reduced inflammatory responses in primary microglia. ORlistat efficiently inhibits murine ATGL and HSL as well as human DAG lipase α, MAGL and the α/β-hydrolase domain 6 ABHD6 (Iglesias et al., 2016). As such, ORlistat has the potential to inhibit the three consecutive steps of TG hydrolysis in murine cells. In contrast, ATGListatin is highly specific to murine ATGL (Iglesias et al., 2016; Zechner et al., 2009). The fact that ATGListatin and ATGL knockdown recapitulated the effect of ORlistat on pro-inflammatory cytokines strongly suggests that the first committed step of TG lipolysis is responsible for the reduced pro-inflammatory responses in microglia. Further, this suggests that reduced ATGL activity is not compensated for by HSL or other lipases as suggested by previous report (Han et al., 2020).

Despite a similar decrease of LPS-induced IL-6, IL-1β and CCL2 expression by ORlistat and ATGListatin in primary microglia, TNF-α expression and secretion remained unchanged. This finding suggests that TG lipolysis regulates the expression of specific pro-inflammatory cytokines in microglia, in agreement with previous studies in co-cultures of macrophages and adipocytes (Xu et al., 2021). However, we cannot rule out that LPS-induced TNF-α expression may be affected at other time points by ORlistat or ATGListatin as recently shown in primary microglia in response to a 24 h treatment with LPS and ATGListatin (Li et al., 2023). Our data demonstrates that inhibition of TG lipolysis downregulates inflammatory responses to LPS in neonatal microglia in a manner similar to previous observations in neonatal microglia (Li et al., 2023), macrophages and neutrophils (Schlager et al., 2015; van Dierendonck et al., 2022). We were able to recapitulate this in cultures of adult microglia. This suggests that ATGL plays a conserved role in the mitigation of inflammation during acute pro-inflammatory insults in peripheral and brain immune cells.

ATGL loss-of-function in microglia reduced LPS-induced IL-1β and IL-6 expression in the hypothalamus and cortex without affecting responses in the hippocampus. Consistent with reduced cytokines response to LPS, the density of IBA1 + cells in the hypothalamus and cortex, in addition to soma size of IBA1 + hypothalamic cells, was also

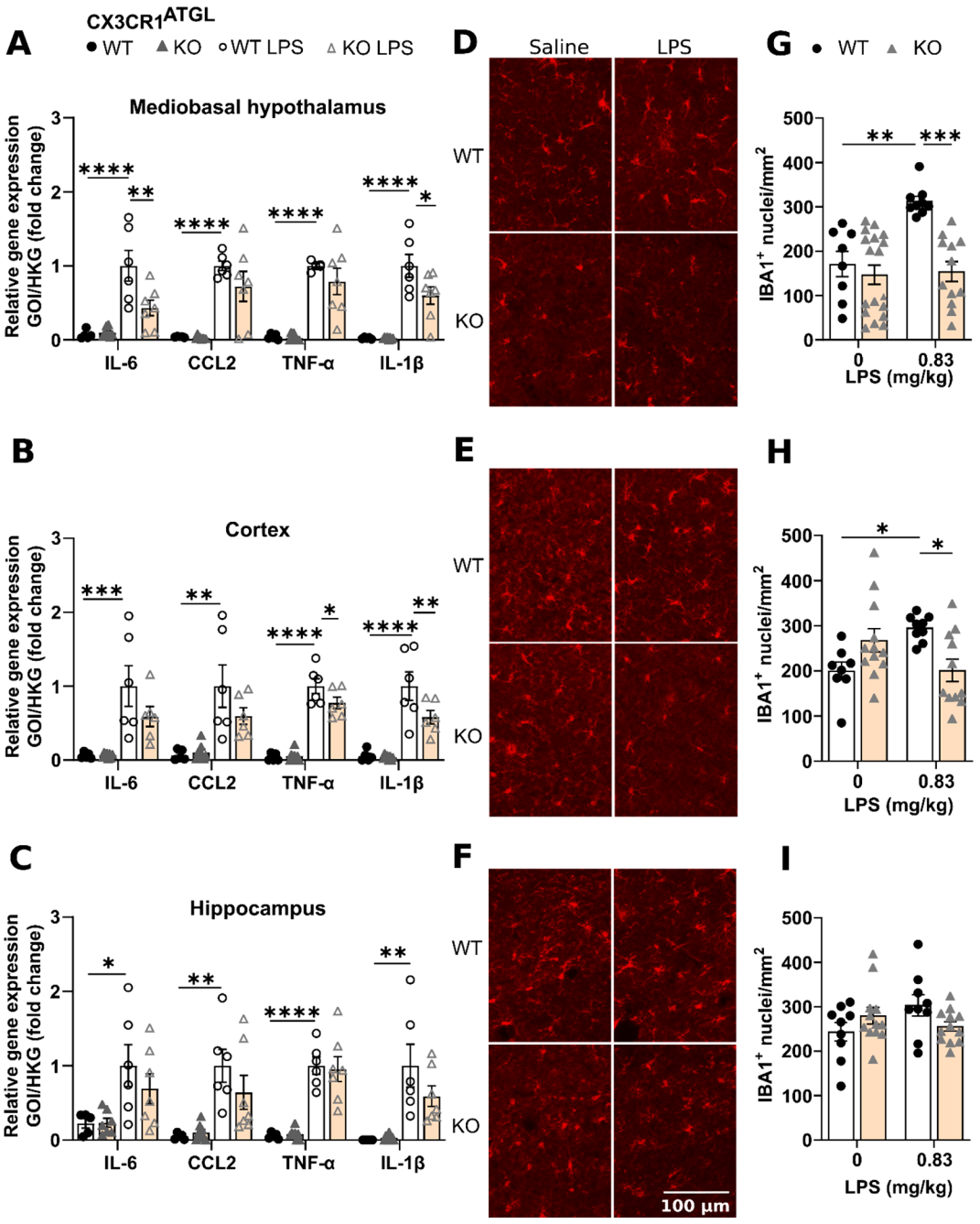

Fig. 7. Loss of microglial ATGL reduces LPS-induced inflammation and microglia density in a brain region-dependent manner. Impact of microglial ATGL loss-of-function (CX3CR1^{ATGL}KO) on LPS-induced cytokine expression and IBA1^{+} microglia density in mouse brain regions compared to Cre-expressing male littermates (CX3CR1^{ATGL}WT). Relative gene expression in the **A.** mediobasal hypothalamus, **B.** cortex and **C.** hippocampus, 3 h after 0.83 mg/kg LPS or saline *i.p.* (n = 6–8 mice/group). IBA1^{+} cells 14 h after LPS (0.83 mg/kg) or saline *i.p.* administration in the **D & G.** mediobasal hypothalamus, **E & H.** cortex and **F & I.** hippocampus, representative images and analysis respectively. 100 µm scale, n = 3–4 mice/group. Two-way ANOVA with post-hoc Šídák. * $p < 0.05$; ** $p < 0.01$; *** $p < 0.001$; **** $p < 0.0001$.

decreased in CX3CR1^{ATGL} KO male mice.

Although inhibition or loss of ATGL led to similar changes in the expression of LPS-induced pro-inflammatory cytokines *in vitro* and *in vivo*, there are limitations in comparing results from both models and in the interpretation of ATGL actions on inflammatory responses. First, whether or not LPS administration acutely induces LD accumulation in microglia *in vivo* remains to be tested. Indeed, while LD accumulation in microglia has been observed several days after LPS administration, changes in LD were not assessed few hours (3–12 h) after *i.p.* LPS (Marschallinger et al., 2020). Second, as the brain samples included all cell types in which LPS promotes pro-inflammatory cytokines, the response originating specifically from microglia remains to be determined. Third, LPS-induced neuroinflammation *in vivo* implicates different integrated pathways (e.g. peripheral cytokines) that are not present in a single cell system. Forth, ATGL inhibition did not affect LPS-induced expression of iNOS and COX2, which are common markers of pro-inflammatory responses in microglia to suggest that ATGL only modulates some LPS-induced pro-inflammatory pathways but not all. Finally, although our data suggest reduced LPS-induced pro-inflammatory signals, the effect of ATGL inhibition on anti-inflammatory

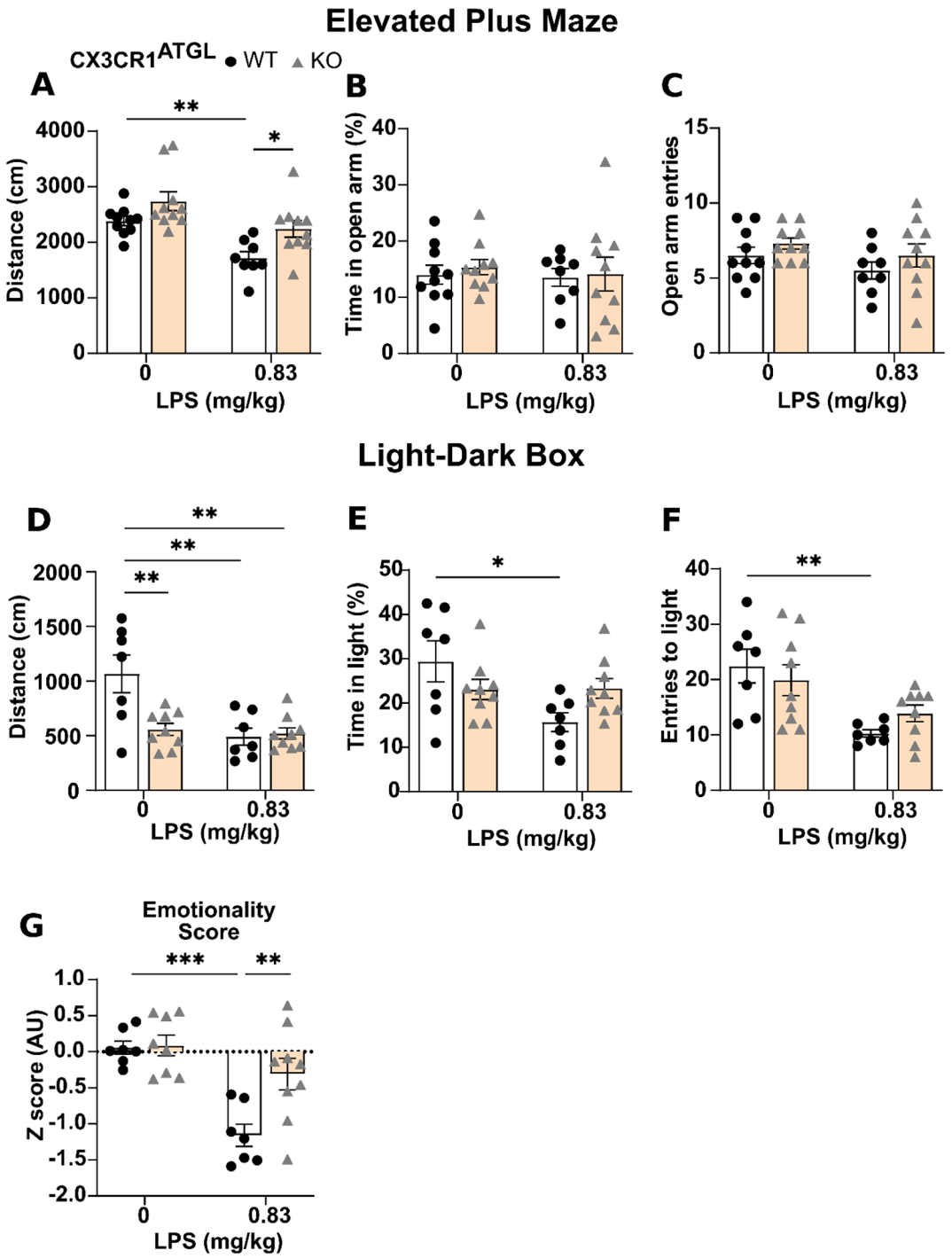

Fig. 8. Loss of ATGL in microglia dampens the behavioural responses to LPS in male mice. Impact of microglial ATGL loss-of-function (CX3CR1^{ATGL}KO) on LPS-induced sickness- and anxiety-like behaviours vs. CX3CR1^{ATGL}WT male littermates (12 h after LPS (0.83 mg/kg) or saline *i.p.*; n = 8–10 mice/group). Measures of **A.** distance travelled, **B.** percentage of total time spent in open arms, and **C.** open arm entries in elevated plus maze during 5 min. Measures of **D.** distance travelled **E.** percentage of total time spent in light, and **F.** entries in the light section of a light–dark box during 5 min. **G.** Emotionality score. Two-way ANOVA with post-hoc Šídák. * $p < 0.05$; ** $p < 0.01$; *** $p < 0.001$; **** $p < 0.0001$.

cytokines *in vitro* was less clear with increased expression of IL-10 contrasting with reduced expression of TGF-β in neonatal cultures. In adult cultures, IL-10 was downregulated while TGF-β was not affected by ATGL inhibition to suggest that regulation of anti-inflammatory signals by ATGL may be affected by the type of microglia culture. Thus, additional studies will be needed to fully evaluate the role of ATGL in regulating microglia function and the balance between anti- and pro-inflammatory responses.

Importantly, reduced inflammatory responses in CX3CR1^{ATGL} KO mice were associated with changes in behavioural disturbances induced by LPS including sickness- and anxiety-like behaviour, consistent with the known effect of IL-6 and IL-1β on anxio-depressive behaviours (Song et al., 2020; Ting et al., 2020). The suppressive effect of LPS on locomotor activity was strongly and consistently reduced in CX3CR1^{ATGL} KO male mice during the EPM and LDB tests. In addition, CX3CR1^{ATGL} KO mice were protected from LPS-induced anxiety as suggested by the lack

of response on number of entries and time in the lit zone during the LDB test. Overall, our findings *in vitro* and *in vivo* provide evidence that inhibition or loss of microglial ATGL activity has protective actions on acute neuroimmune and behavioural disturbances induced by LPS. Mitigation of neuroimmune responses by ATGL may extend to other types of brain insults as suggested by a recent study reporting that brain-restricted administration of ATGListatin reduces neural damages induced by stroke in mice (Li et al., 2023).

One potential pathway underlying ATGL actions on microglial LPS responses may be reduced release and availability of fatty acids for mitochondrial oxidation. ATGL inhibition reduced FAO in a manner similar to etomoxir, demonstrating that basal ATGL-dependent lipolysis in microglia generates substrates for FAO. However, FAO inhibition with etomoxir did not recapitulate the effect of ATGListatin on LPS-induced CCL2 expression (6 h) and IL-6 and CCL2 secretion (24 h). These results strongly suggest that the anti-inflammatory actions of ATGL inhibition do not rely on FAO and that FAO does not modulate inflammatory responses to LPS in these experimental conditions. These results are in contrast with a recent study showing that etomoxir exacerbates pro-inflammatory responses in microglia activated by myelin debris (Qin et al., 2023). Such difference could be related to different types of stimuli (LPS vs. myelin debris) and associated signalling pathways.

Based on our findings, we speculated that ATGL may regulate the generation of fatty-acid-derived inflammatory signals including prostanoids which are metabolites of arachidonic acid. Using targeted oxylipin profiling, we found that ATGL inhibition led to a strong decrease of LPS-induced PGE2, PGD_2 and TXB2 secretion and intracellular PGF2α level. The expression of COX2, a key enzyme required for prostanoid synthesis, was not affected by ATGL inhibition in presence of LPS. This therefore suggests that ATGL inhibition may reduce the release of arachidonic acid from LD during LPS treatment thereby decreasing prostanoid synthesis. These findings are in agreement with studies reporting that ATGL inhibition or loss-of-function reduces prostanoid synthesis under inflammatory conditions in macrophages (van Dierendonck et al., 2022) and neutrophils (Schlager et al., 2015). Prostanoids, particularly PGE_2, activate transcription factors promoting the synthesis of IL-6 and other cytokines (Fiebich et al., 2001; Kawahara et al., 2015; Ricciotti & Fitzgerald, 2011). This raises the possibility that mitigation of LPS-induced cytokine responses by ATGL inhibition are secondary to reduced prostanoid signalling.

The broader impact of ATGL inhibition on the microglial lipidome was assessed using untargeted lipidomics. Of the identified lipid species, ceramides were the only species significantly affected by LPS and/or ATGL inhibition. ATGListatin increased the level of dihydroceramides 18:0/24:0 and 18:0/24:1 while reducing ceramide 18:1/24:0 and 18:1/24:1 levels. LPS treatment showed a similar pattern, though less pronounced, on dihydroceramide and ceramide levels which was exacerbated by ATGL inhibition. ATGListatin also increased sphingomyelin d18:0/18:0 in presence of LPS compared to LPS alone. *De novo* synthesis of ceramides starts with palmitoyl-CoA derived from palmitate, which generates dihydroceramides after a series of enzymatic reactions. These dihydroceramides act as precursors for ceramide synthesis by the enzyme Δ4-dihydroceramide desaturase 1 (DEGS1) (Tzou et al., 2023). If ATGL activity releases palmitate acting as a precursor for ceramide synthesis, one would expect that ATGL inhibition would reduce dihydroceramide synthesis. Given that the opposite is observed on dihydroceramide levels, we speculate that ATGL inhibition reduces activity of DEGS1. This would result in the observed increase in dihydroceramide and decreased ceramide levels.

It is also possible, and not exclusive, that the reduced ceramide level may result from decreased sphingomyelinase activity. This is supported by increased SM 18:0/18:0 level in response to LPS and ATGListatin. Although it is difficult to identify the specific pathway(s) underlying these changes and to establish a causal relationship between ceramide levels and/or subtypes, and the inflammatory profile, our findings show for the first time that ATGL regulates ceramide subclasses in microglia including dihydroceramides which are now recognized as bioactive molecules with immunomodulatory properties (Lachkar et al., 2021). The decreased ceramide levels reported here contrasts with the accumulation of deleterious ceramides reported in ATGL deficient macrophages (Aflaki et al., 2012) and cardiomyocytes (Gao et al., 2015) to suggest that regulation of ceramides by ATGL is cell specific.

Whether or not changes in microglial dihydroceramide and ceramide levels are secondary to decreased prostanoids and cytokines signalling will require additional studies. Overall, the current lipidomic results demonstrate that the dampened pro-inflammatory profile induced by ATGL inhibition in microglia is associated with reduced levels of pro-inflammatory prostanoids and ceramides. Our lipidome and LD data somehow contrast with a recent study showing that the knock-down of lipoprotein lipase (LPL) in microglia induces LD accumulation associated with a pro-inflammatory polarization and a profound remodeling of the lipidome in basal conditions in BV-2 microglia (Loving et al., 2021). Several lipid classes including cholesterol esters and phospholipids, and their saturation degree, were altered by LPL downregulation. While there is not a consistent association between LD accumulation and the inflammatory state when comparing both studies, LPL and ATGL play different roles in lipid metabolism. LPL is the main enzyme catalysing the hydrolysis of fatty-acids esterified in circulating TG-rich lipoproteins, a process by which it regulates fatty-acids uptake in microglia (Bruce et al., 2018). As such, LPL downregulation reduces fatty acid availability at large in microglia leading to major changes in lipid distribution, composition, metabolism and signalling that promote pro-inflammatory responses (Loving et al., 2021). Whether this change in lipid availability triggers or results from LD accumulation remains to be elucidated. On the other hand, ATGL specifically regulates the availability of intracellular fatty-acids stored in LD, and while ATGL inhibition acutely increased LD number, it did not affect dramatically lipid composition or microglia pro-inflammatory profile (e.g. cytokines and prostanoids) in basal conditions. Together these findings suggest that the association between LD accumulation and pro-inflammatory polarization may be context dependant.

Our findings, in line with recent studies (Li et al., 2023) strongly suggest that inhibition of ATGL-dependent TG hydrolysis in microglia reduces the acute microglial pro-inflammatory response *in vitro* and *in vivo*. In addition, LD accumulation induced by ATGL inhibition was associated with increased phagocytosis. These results contrast with studies showing aging, Alzheimer's and neurodegenerative diseases or other type of brain insults (e.g. traumatic brain injury) are associated with LD accumulation, pro-inflammatory responses and impaired phagocytosis in microglia (Arbaizar-Rovirosa et al., 2023; Claes et al., 2021; Lee et al., 2023; Marschallinger et al., 2020; Zambusi et al., 2022; Li et al., 2024). These differences may be related to the duration or nature of insults.

We realize that it seems paradoxical that LPS and ATGL inhibition, which both acutely induce LD accumulation, have different effects on pro-inflammatory cytokines. There are however several aspects that may underlie this discrepancy. First, increased LD number in response to ATGL inhibition does not affect expression and secretion of cytokines, nor prostanoid levels, in basal conditions (no LPS) thereby suggesting that acute LD accumulation is not sufficient to modulate pro-inflammatory markers. This idea is supported by our data in mice showing that microglial ATGL deficiency does not affect cytokine expression, microglia density and soma size or anxiety-like behaviors in basal conditions. Second, it is important to not only consider the number of LD but also the dynamics of LD formation and hydrolysis. Indeed, while ATGL inhibition increases LD number by blocking hydrolysis and fatty-acid release, and LPS reduces ATGL expression favoring LD accumulation, we cannot rule out that LPS also increases fatty-acid esterification in LD and thus "trap" fatty-acids that regulate inflammatory responses. Third, it is possible that LPS-induced ATGL downregulation and LD accumulation are pathways acutely activated to mitigate LPS-induced pro-inflammatory cytokines and ceramides, an effect further

enhanced by inhibition of residual ATGL. Finally, it is conceivable that acute pro-inflammatory insults increase LD number which mitigates inflammation but that chronic accumulation of LD in microglia promotes or aggravates neuroinflammation in response to insults. Further studies are warranted to better understand the role of ATGL-dependent LD lipolysis in regulating microglia function in a time resolved manner. In addition, considering the strong sex differences in microglia metabolism and activation (Cleland et al., 2024; Han et al., 2021), it will be important to assess if ATGL differently regulates microglial function in males and females.

Collectively, our findings identify ATGL as a regulator of microglia reactivity and neuroinflammation during acute inflammatory insults that may have implications for our understanding of the pathways regulating microglia activity in physiological and pathophysiological states. Further studies will be required to elucidate the role of microglial ATGL and LD lipolysis in CNS pathologies associated with chronic neuroinflammation and microglial activation such as mood disorder, obesity and Alzheimer's.

CRediT authorship contribution statement

Josephine Louise Robb: Writing – review & editing, Writing – original draft, Visualization, Supervision, Methodology, Investigation, Formal analysis, Data curation, Conceptualization. **Frédérick Boisjoly:** Methodology, Investigation, Data curation. **Arturo Israel Machuca-Parra:** Methodology, Investigation, Conceptualization. **Adeline Coursan:** Methodology, Investigation, Data curation. **Romane Manceau:** Writing – review & editing, Methodology, Investigation. **Danie Majeur:** Writing – review & editing, Methodology, Investigation. **Demetra Rodaros:** Resources, Methodology, Investigation. **Khalil Bouyakdan:** Writing – review & editing, Methodology, Investigation. **Karine Greffard:** Investigation, Data curation. **Jean-François Bilodeau:** Writing – review & editing, Methodology, Investigation, Conceptualization. **Anik Forest:** Visualization, Methodology, Investigation, Data curation. **Caroline Daneault:** Visualization, Methodology, Investigation, Data curation. **Matthieu Ruiz:** Writing – review & editing, Methodology, Investigation, Formal analysis, Conceptualization. **Cyril Laurent:** Methodology, Investigation. **Nathalie Arbour:** Writing – review & editing, Methodology, Investigation. **Sophie Layé:** Writing – review & editing, Methodology, Conceptualization. **Xavier Fioramonti:** Writing – review & editing, Methodology, Investigation, Formal analysis, Conceptualization. **Charlotte Madore:** Writing – review & editing, Methodology, Investigation, Formal analysis. **Stephanie Fulton:** Writing – review & editing, Supervision, Resources, Methodology, Formal analysis, Conceptualization. **Thierry Alquier:** Writing – review & editing, Writing – original draft, Validation, Supervision, Resources, Project administration, Methodology, Investigation, Funding acquisition, Formal analysis, Data curation, Conceptualization.

Declaration of Competing Interest

The authors declare that they have no known competing financial interests or personal relationships that could have appeared to influence the work reported in this paper.

Data availability

Data will be made available on request.

Acknowledgements

We are grateful to Dr Grant Mitchell for the ATGL-floxed mice. We thank the CRCHUM cytometry core facility for their help with FACS studies and the cellular imaging core facility. This work was supported by grants from the National Natural Sciences and Engineering Research Council (NSERC, RGPIN/04798), the Canadian Institutes of Health Research (CIHR, PJT153035) and Réseau de recherche en santé cardiométabolique, diabète & obésité from Fonds de Recherche Québec-Santé (CMDO-FRQS) to T.A., a CIHR grant (PJT169015) to S.F. and T.A., and grants from Fondation pour la Recherche Médicale (FRM, France), Fédération pour la Recherche sur le Cerveau (FRC, France) and Institut Benjamin Delessert (France) to X.F.. A.C. was supported by a fellowship from INRAE/Bordeaux INP (France). C.M. was supported by a post-doctoral award from AgreenSkills. S.F., M.R. and T.A. were supported by a salary award from FRQS. J.L.R., R.M, D.M. and F.B. were supported by doctoral and postdoctoral FRQS fellowships, PhD fellowships from the Neuroscience Department and MSc fellowship from CRCHUM. A.I.M.P was supported by a fellowship from Montreal Diabetes Research Center and Faculty of Medicine. C.L. obtained postdoctoral awards from Fondation d'Aide pour la Recherche sur la Sclérose en Plaques (ARSEP), FRQS and CIHR.

Author's contributions

J.L.R., A.I.M.P, F.B., R.M., D.M., D.R, K.B., A.C. and C.L. helped with colony management and genotyping, cell culture, qPCR, ELISA, fatty acid oxidation, histology and imaging, FACS experiments and behaviour tests. M.R., A.F. and C.D. carried out LC-MS/MS for untargeted lipidomics, data analysis and interpretation, and contributed to manuscript preparation. K.G. and J.-F.B. carried out LC-MS/MS for targeted lipidomics, data analysis and contributed to manuscript preparation. J.L.R., A.I.M.P., F.B., D.M., K.B., X. F., C.M.-D., S.L., N.A., S.F. and T.A. contributed to conceptualization, experimental design, data interpretation and manuscript revisions. J.L.R. and T.A. wrote the manuscript.

Ethics approval

All animal studies were conducted in accordance with guidelines of the Canadian Council on Animal Care and the Institutional Animal Care Committee of CRCHUM (protocol #CM19018TAs and CM23041TAs) and in accordance with the European directive 2010/63/UE and approved by the French Ministry of Research and local ethics committees (APAFIS#: 33951).

Appendix A. Supplementary data

Supplementary data to this article can be found online at https://doi.org/10.1016/j.bbi.2024.09.027.

References

Aflaki, E., Balenga, N.A.B., Luschnig-Schratl, P., Wolinski, H., Povoden, S., Chandak, P. G., Bogner-Strauss, J.G., Eder, S., Konya, V., Kohlwein, S.D., Heinemann, A., Kratky, D., 2011. Impaired Rho GTPase activation abrogates cell polarization and migration in macrophages with defective lipolysis. Cell Mol Life Sci 68 (23), 3933. https://doi.org/10.1007/S00018-011-0688-4.

Aflaki, E., Doddapattar, P., Radović, B., Povoden, S., Kolb, D., Vujić, N., Wegscheider, M., Koefeler, H., Hornemann, T., Graier, W.F., Malli, R., Madeo, F., Kratky, D., 2012. C16 ceramide is crucial for triacylglycerol-induced apoptosis in macrophages. Cell Death Dis 3 (3). https://doi.org/10.1038/CDDIS.2012.17.

Arbaizar-Rovirosa, M., Pedragosa, J., Lozano, J.J., Casal, C., Pol, A., Gallizioli, M., Planas, A.M., 2023. Aged lipid-laden microglia display impaired responses to stroke. EMBO Mol Med 15 (2). https://doi.org/10.15252/EMMM.202217175.

Becskei, C., Riediger, T., Hernádfalvy, N., Arsenijevic, D., Lutz, T.A., Langhans, W., 2008. Inhibitory effects of lipopolysaccharide on hypothalamic nuclei implicated in the control of food intake. Brain Behav Immun 22 (1), 56–64. https://doi.org/10.1016/J.BBI.2007.06.002.

Bilodeau, J.F., Gevariya, N., Larose, J., Robitaille, K., Roy, J., Oger, C., Galano, J.M., Bergeron, A., Durand, T., Fradet, Y., Julien, P., Fradet, V., 2021. Long chain omega-3 fatty acids and their oxidized metabolites are associated with reduced prostate tumor growth. Prostaglandins Leukot Essent Fat Acids 164. https://doi.org/10.1016/J.PLEFA.2020.102215.

Bruce, K.D., Gorkhali, S., Given, K., Coates, A.M., Boyle, K.E., Macklin, W.B., Eckel, R.H., 2018. Lipoprotein Lipase Is a Feature of Alternatively-Activated Microglia and May Facilitate Lipid Uptake in the CNS During Demyelination. Front Mol Neurosci 11. https://doi.org/10.3389/FNMOL.2018.00057.

Brymer, K.J., Romay-Tallon, R., Allen, J., Caruncho, H.J., Kalynchuk, L.E., 2019. Exploring the Potential Antidepressant Mechanisms of TNFα Antagonists. Front Neurosci 13 (FEB). https://doi.org/10.3389/FNINS.2019.00098.

Butovsky, O., Jedrychowski, M.P., Moore, C.S., Cialic, R., Lanser, A.J., Gabriely, G., Koeglsperger, T., Dake, B., Wu, P.M., Doykan, C.E., Fanek, Z., Liu, L., Chen, Z., Rothstein, J.D., Ransohoff, R.M., Gygi, S.P., Antel, J.P., Weiner, H.L., 2014. Identification of a Unique TGF-β Dependent Molecular and Functional Signature in Microglia. Nat Neurosci 17 (1), 131. https://doi.org/10.1038/NN.3599.

Capuron, L., Miller, A.H., 2011. Immune System to Brain Signaling: Neuropsychopharmacological Implications. Pharmacol Ther 130 (2), 226. https://doi.org/10.1016/J.PHARMTHERA.2011.01.014.

Claes, C., Danhash, E.P., Hasselmann, J., Chadarevian, J.P., Shabestari, S.K., England, W. E., Lim, T.E., Hidalgo, J.L.S., Spitale, R.C., Davtyan, H., Blurton-Jones, M., 2021. Plaque-associated human microglia accumulate lipid droplets in a chimeric model of Alzheimer's disease. Mol Neurodegener 16 (1). https://doi.org/10.1186/S13024-021-00473-0.

Cleland, N.R.W., Potter, G.J., Buck, C., Quang, D., Oldham, D., Neal, M., Saviola, A., Niemeyer, C.S., Dobrinskikh, E., Bruce, K.D., 2024. Altered metabolism and DAM-signatures in female brains and microglia with aging. Brain Res 1829, 148772. https://doi.org/10.1016/J.BRAINRES.2024.148772.

Demers, G., Roy, J., Machuca-Parra, A. I., Dashtehei pour, Z., Bairamian, D., Daneault, C., Rosiers, C. Des, Ferreira, G., Alquier, T., & Fulton, S. (2020). Fish oil supplementation alleviates metabolic and anxiodepressive effects of diet-induced obesity and associated changes in brain lipid composition in mice. *International Journal of Obesity*, *44*(9), 1936–1945. doi: 10.1038/S41366-020-0623-6.

Dort, J., Orfi, Z., Fabre, P., Molina, T., Conte, T.C., Greffard, K., Pellerito, O., Bilodeau, J. F., Dumont, N.A., 2021. Resolvin-D2 targets myogenic cells and improves muscle regeneration in Duchenne muscular dystrophy. Nat Commun 12 (1). https://doi.org/10.1038/S41467-021-26516-0.

Eichmann, T.O., Kumari, M., Haas, J.T., Farese, R.V., Zimmermann, R., Lass, A., Zechner, R., 2012. Studies on the Substrate and Stereo/Regioselectivity of Adipose Triglyceride Lipase, Hormone-sensitive Lipase, and Diacylglycerol-O-acyltransferases. J Biol Chem 287 (49), 41446. https://doi.org/10.1074/JBC.M112.400416.

Eichmann, T.O., Lass, A., 2015. DAG tales: the multiple faces of diacylglycerol—stereochemistry, metabolism, and signaling. Cell Mol Life Sci 72 (20), 3931. https://doi.org/10.1007/S00018-015-1982-3.

Feingold, K.R., Shigenaga, J.K., Kazemi, M.R., McDonald, C.M., Patzek, S.M., Cross, A.S., Moser, A., Grunfeld, C., 2012. Mechanisms of triglyceride accumulation in activated macrophages. J Leukoc Biol 92 (4), 829. https://doi.org/10.1189/JLB.1111537.

Fiebich, B.L., Schleicher, S., Spleiss, O., Czygan, M., Hüll, M., 2001. Mechanisms of prostaglandin E2-induced interleukin-6 release in astrocytes: Possible involvement of EP4-like receptors, p38 mitogen-activated protein kinase and protein kinase C. J Neurochem 79 (5), 950–958. https://doi.org/10.1046/J.1471-4159.2001.00652.X.

Forest, A., Ruiz, M., Bouchard, B., Boucher, G., Gingras, O., Daneault, C., Robillard Frayne, I., Rhainds, D., Tardif, J.C., Rioux, J.D., Des Rosiers, C., 2018. A Comprehensive and Reproducible Untargeted Lipidomic Workflow Using LC-QTOF Validated for Human Plasma Analysis. J Proteome Res 17 (11), 3657. https://doi.org/10.1021/ACS.JPROTEOME.8B00270.

Gao, H., Feng, X.J., Li, Z.M., Li, M., Gao, S., He, Y.H., Wang, J.J., Zeng, S.Y., Liu, X.P., Huang, X.Y., Chen, S.R., Liu, P.Q., 2015. Downregulation of adipose triglyceride lipase promotes cardiomyocyte hypertrophy by triggering the accumulation of ceramides. Arch Biochem Biophys 565, 76–88. https://doi.org/10.1016/J.ABB.2014.11.009.

Ghasemi, M., Navidhamidi, M., Rezaei, F., Azizikia, A., Mehranfard, N., 2022. Anxiety and hippocampal neuronal activity: Relationship and potential mechanisms. Cogn Affect Behav Neurosci 22 (3), 431–449. https://doi.org/10.3758/S13415-021-00973-Y.

Guilloux, J.P., Seney, M., Edgar, N., Sibille, E., 2011. Integrated behavioral z-scoring increases the sensitivity and reliability of behavioral phenotyping in mice: Relevance to emotionality and sex. J Neurosci Methods 197 (1), 21–31. https://doi.org/10.1016/j.jneumeth.2011.01.019.

Han, S. L., Liu, Y., Limbu, S. M., Chen, L. Q., Zhang, M. L., & Du, Z. Y. (2020). The reduction of lipid-sourced energy production caused by ATGL inhibition cannot be compensated by activation of HSL, autophagy, and utilization of other nutrients in fish. *Fish Physiology and Biochemistry 2020 47:1*, *47*(1), 173–188. doi: 10.1007/S10695-020-00904-7.

Han, J., Fan, Y., Zhou, K., Blomgren, K., Harris, R.A., 2021. Uncovering sex differences of rodent microglia. J Neuroinflammation 18 (1). https://doi.org/10.1186/S12974-021-02124-Z.

Herron, S., Delpech, J.C., Madore, C., Ikezu, T., 2022. Using mechanical homogenization to isolate microglia from mouse brain tissue to preserve transcriptomic integrity. STAR Protocols 3 (4). https://doi.org/10.1016/J.XPRO.2022.101670.

Huang, Y.L., Morales-Rosado, J., Ray, J., Myers, T.G., Kho, T., Lu, M., Munford, R.S., 2014. Toll-like receptor agonists promote prolonged triglyceride storage in macrophages. J Biol Chem 289 (5), 3001–3012. https://doi.org/10.1074/JBC.M113.524587.

Iglesias, J., Lamontagne, J., Erb, H., Gezzar, S., Zhao, S., Joly, E., Truong, V.L., Skorey, K., Crane, S., Madiraju, S.R.M., Prentki, M., 2016. Simplified assays of lipolysis enzymes for drug discovery and specificity assessment of known inhibitors. J Lipid Res 57 (1), 131–141. https://doi.org/10.1194/JLR.D058438.

Itabe, H., Yamaguchi, T., Nimura, S., Sasabe, N., 2017. Perilipins: a diversity of intracellular lipid droplet proteins. Lipids Health Dis 16 (1). https://doi.org/10.1186/s12944-017-0473-y.

Jarc, E., Petan, T., 2020. A twist of FATe: Lipid droplets and inflammatory lipid mediators. Biochimie 169, 69–87. https://doi.org/10.1016/J.BIOCHI.2019.11.016.

Jha, P., Claudel, T., Baghdasaryan, A., Mueller, M., Halilbasic, E., Das, S.K., Lass, A., Zimmermann, R., Zechner, R., Hoefler, G., Trauner, M., 2014. Role of adipose triglyceride lipase (PNPLA2) in protection from hepatic inflammation in mouse models of steatohepatitis and endotoxemia. Hepatology 59 (3), 858–869. https://doi.org/10.1002/HEP.26732.

Kawahara, K., Hohjoh, H., Inazumi, T., Tsuchiya, S., Sugimoto, Y., 2015. Prostaglandin E2-Induced Inflammation: Relevance of Prostaglandin e Receptors. in *Biochimica et Biophysica Acta - Molecular and Cell Biology of Lipids* Vol. 1851(4, 414–421.

Khatchadourian, A., Bourque, S.D., Richard, V.R., Titorenko, V.I., Maysinger, D., 2012. Dynamics and regulation of lipid droplet formation in lipopolysaccharide (LPS)-stimulated microglia. *Biochimica et Biophysica Acta (BBA) - Molecular and Cell Biology of*. Lipids 1821 (4), 607–617. https://doi.org/10.1016/J.BBALIP.2012.01.007.

Kotzbeck, P., Giordano, A., Mondini, E., Murano, I., Severi, I., Venema, W., Cecchini, M. P., Kershaw, E.E., Barbatelli, G., Haemmerle, G., Zechner, R., Cinti, S., 2018. Brown adipose tissue whitening leads to brown adipocyte death and adipose tissue inflammation. J Lipid Res 59 (5), 784. https://doi.org/10.1194/JLR.M079665.

Lachkar, F., Ferre, P., Foufelle, F., Papaioannou, A., 2021. Dihydroceramides: their emerging physiological roles and functions in cancer and metabolic diseases. Am J Phys Endocrinol Metab 320 (1), E122–E130. https://doi.org/10.1152/AJPENDO.00330.2020.

Lammers, B., Chandak, P.G., Aflaki, E., Van Puijvelde, G.H.M., Radovic, B., Hildebrand, R.B., Meurs, I., Out, R., Kuiper, J., Van Berkel, T.J.C., Kolb, D., Haemmerle, G., Zechner, R., Levak-Frank, S., Van Eck, M., Kratky, D., 2011. Macrophage Adipose Triglyceride Lipase Deficiency Attenuates Atherosclerotic Lesion Development in Low-Density Lipoprotein Receptor Knockout Mice. Arterioscler Thromb Vasc Biol 31 (1), 67. https://doi.org/10.1161/ATVBAHA.110.215814.

Lee, J., Dimitry, J.M., Song, J.H., Son, M., Sheehan, P.W., King, M.W., Travis Tabor, G., Goo, Y.A., Lazar, M.A., Petrucelli, L., Musiek, E.S., 2023. Microglial REV-ERBα regulates inflammation and lipid droplet formation to drive tauopathy in male mice. *Nature*. Communications 14 (1). https://doi.org/10.1038/S41467-023-40927-1.

Lefort, B., Gélinas, R., Forest, A., Bouchard, B., Daneault, C., Robillard Frayne, I., Roy, J., Oger, C., Greffard, K., Galano, J.M., Durand, T., Labarthe, F., Bilodeau, J.F., Ruiz, M., Des Rosiers, C., 2023. Remodeling of lipid landscape in high fat fed very-long chain acyl-CoA dehydrogenase null mice favors pro-arrhythmic polyunsaturated fatty acids and their downstream metabolites. Biochim Biophys Acta (BBA) - Mol Basis Dis 1869 (8), 166843. https://doi.org/10.1016/J.BBADIS.2023.166843.

Legroux, L., Pittet, C.L., Beauseigle, D., Deblois, G., Prat, A., Arbour, N., 2015. An optimized method to process mouse CNS to simultaneously analyze neural cells and leukocytes by flow cytometry. J Neurosci Methods 247, 23–31. https://doi.org/10.1016/J.JNEUMETH.2015.03.021.

Lettieri Barbato, D., Aquilano, K., Baldelli, S., Cannata, S.M., Bernardini, S., Rotilio, G., Ciriolo, M.R., 2014a. Proline oxidase–adipose triglyceride lipase pathway restrains adipose cell death and tissue inflammation. Cell Death Differ 21 (1), 113. https://doi.org/10.1038/CDD.2013.137.

Lettieri Barbato, D., Tatulli, G., Aquilano, K., Ciriolo, M.R., 2014b. Inhibition of Age-Related Cytokines Production by ATGL: A Mechanism Linked to the Anti-Inflammatory Effect of Resveratrol. Mediators Inflamm 2014. https://doi.org/10.1155/2014/917698.

Li, H., Liu, P., Deng, S., Zhu, L., Cao, X., Bao, X., Xia, S., Xu, Y., Zhang, B., 2023. Pharmacological Upregulation of Microglial Lipid Droplet Alleviates Neuroinflammation and Acute Ischemic Brain Injury. Inflammation 46 (5), 1832. https://doi.org/10.1007/S10753-023-01844-Z.

Li, Y., Munoz-Mayorga, D., Nie, Y., Kang, N., Tao, Y., Lagerwall, J., Pernaci, C., Curtin, G., Coufal, N.G., Mertens, J., Shi, L., Chen, X., 2024. Microglial lipid droplet accumulation in tauopathy brain is regulated by neuronal AMPK. Cell Metab 36 (6). https://doi.org/10.1016/J.CMET.2024.03.014.

Littman, D., 2013. An inducible cre recombinase driven by Cx3cr1. MGI Direct Data Submission. https://www.informatics.jax.org/reference/J:190965.

Loving, B.A., Tang, M., Neal, M.C., Gorkhali, S., Murphy, R., Eckel, R.H., Bruce, K.D., 2021. Lipoprotein Lipase Regulates Microglial Lipid Droplet Accumulation. Cells 10 (2), 1–17. https://doi.org/10.3390/CELLS10020198.

Marschallinger, J., Iram, T., Zardeneta, M., Lee, S.E., Lehallier, B., Haney, M.S., Pluvinage, J.V., Mathur, V., Hahn, O., Morgens, D.W., Kim, J., Tevini, J., Felder, T. K., Wolinski, H., Bertozzi, C.R., Bassik, M.C., Aigner, L., Wyss-Coray, T., 2020. Lipid droplet accumulating microglia represent a dysfunctional and pro-inflammatory state in the aging brain. Nat Neurosci 23 (2), 194. https://doi.org/10.1038/S41593-019-0566-1.

Nakajima, S., Demers, G., Machuca-Parra, A.I., Pour, Z.D., Bairamian, D., Bouyakdan, K., Fisette, A., Kabahizi, A., Robb, J., Rodaros, D., Laurent, C., Ferreira, G., Arbour, N., Alquier, T., Fulton, S., 2023. Central activation of the fatty acid sensor GPR120 suppresses microglia reactivity and alleviates sickness- and anxiety-like behaviors. J Neuroinflammation 20 (1), 302. https://doi.org/10.1186/S12974-023-02978-5.

Olzmann, J.A., Carvalho, P., 2019. Dynamics and functions of lipid droplets. Nat Rev Mol Cell Biol 20 (3), 137–155. https://doi.org/10.1038/s41580-018-0085-z.

Parkhurst, C.N., Yang, G., Ninan, I., Savas, J.N., Yates, J.R., Lafaille, J.J., Hempstead, B. L., Littman, D.R., Gan, W.B., 2013. Microglia promote learning-dependent synapse formation through BDNF. Cell 155 (7), 1596. https://doi.org/10.1016/J.CELL.2013.11.030.

Paxinos, G., Franklin, K., 2008. The Mouse Brain in Stereotaxic Coordinates, Compact | 978–0-12-374244-5 | Elsevier. The Mouse Brain in Stereotaxic Coordinates 827–828. https://books.google.com/books/about/The_Mouse_Brain_in_Stereotaxic_Coordinat.html?id=EHy1QN1xv0gC.

Qin, C., Yang, S., Chen, M., Dong, M.H., Zhou, L.Q., Chu, Y.H., Shen, Z.X., Bosco, D.B., Wu, L.J., Tian, D.S., Wang, W., 2023. Modulation of microglial metabolism facilitates regeneration in demyelination. Iscience 26 (5), 106588. https://doi.org/10.1016/J.ISCI.2023.106588.

Ricciotti, E., Fitzgerald, G.A., 2011. Prostaglandins and Inflammation. Arterioscler Thromb Vasc Biol 31, 986–1000. https://doi.org/10.1161/ATVBAHA.110.207449.

Ruiz, M., Cuillerier, A., Daneault, C., Deschênes, S., Frayne, I.R., Bouchard, B., Forest, A., Legault, J.T., Vaz, F.M., Rioux, J.D., Burelle, Y., Rosiers, C.D., 2019. Lipidomics unveils lipid dyshomeostasis and low circulating plasmalogens as biomarkers in a monogenic mitochondrial disorder. *JCI*. Insight 4 (14). https://doi.org/10.1172/JCI.INSIGHT.123231.

Sahasrabuddhe, V., Singhee Ghosh, H., 2022. Cx3Cr1-Cre induction leads to microglial activation and IFN-1 signaling caused by DNA damage in early postnatal brain. Cell Rep 38, 110252. https://doi.org/10.1016/j.celrep.2021.110252.

Savage, J.C., Carrier, M., Tremblay, M.È., 2019. Morphology of Microglia Across Contexts of Health and Disease. Methods Mol Biol 2034, 13–26. https://doi.org/10.1007/978-1-4939-9658-2_2/FIGURES/2.

Schindelin, J., Arganda-Carreras, I., Frise, E., Kaynig, V., Longair, M., Pietzsch, T., Preibisch, S., Rueden, C., Saalfeld, S., Schmid, B., Tinevez, J.-Y., White, D.J., Hartenstein, V., Eliceiri, K., Tomancak, P., Cardona, A., 2012. Fiji: an open-source platform for biological-image analysis. Nat Methods 9, 676. https://doi.org/10.1038/nmeth.2019.

Schlager, S., Goeritzer, M., Jandl, K., Frei, R., Vujic, N., Kolb, D., Strohmaier, H., Dorow, J., Eichmann, T.O., Rosenberger, A., Wolfler, A., Lass, A., Kershaw, E.E., Ceglarek, U., Dichlberger, A., Heinemann, A., Kratky, D., 2015. Adipose triglyceride lipase acts on neutrophil lipid droplets to regulate substrate availability for lipid mediator synthesis. J Leukoc Biol 98 (5), 837–850. https://doi.org/10.1189/JLB.3A0515-206R.

Schneider, C.A., Rasband, W.S., Eliceiri, K.W., 2012. NIH Image to ImageJ: 25 years of image analysis. Nat Methods 9, 671. https://doi.org/10.1038/nmeth.2089.

Sharma, S., & Fulton, S. (2013). Diet-induced obesity promotes depressive-like behaviour that is associated with neural adaptations in brain reward circuitry. *International Journal of Obesity (2005)*, *37*(3), 382–389. doi: 10.1038/IJO.2012.48.

Song, A.Q., Gao, B., Fan, J.J., Zhu, Y.J., Zhou, J., Wang, Y.L., Xu, L.Z., Wu, W.N., Wu, W. N., 2020. NLRP1 inflammasome contributes to chronic stress-induced depressive-like behaviors in mice. J Neuroinflammation 17 (1). https://doi.org/10.1186/S12974-020-01848-8.

Soto-Tinoco, E., Guerrero-Vargas, N.N., Buijs, R.M., 2016. Interaction between the hypothalamus and the immune system. Exp Physiol 101 (12), 1463–1471. https://doi.org/10.1113/EP085560.

Taïb, B., Bouyakdan, K., Hryhorczuk, C., Rodaros, D., Fulton, S., Alquier, T., 2013. Glucose regulates hypothalamic long-chain fatty acid metabolism via AMP-activated kinase (AMPK) in neurons and astrocytes. J Biol Chem 288 (52), 37216–37229. https://doi.org/10.1074/jbc.M113.506238.

Ting, E.Y.C., Yang, A.C., Tsai, S.J., 2020. Role of Interleukin-6 in Depressive Disorder. Int J Mol Sci 21 (6). https://doi.org/10.3390/IJMS21062194.

Tzou, F.Y., Hornemann, T., Yeh, J.Y., Huang, S.Y., 2023. The pathophysiological role of dihydroceramide desaturase in the nervous system. Prog Lipid Res 91. https://doi.org/10.1016/J.PLIPRES.2023.101236.

van Dierendonck, X.A.M.H., Vrieling, F., Smeehuijzen, L., Deng, L., Boogaard, J.P., Croes, C.A., Temmerman, L., Wetzels, S., Biessen, E., Kersten, S., Stienstra, R., 2022. Triglyceride breakdown from lipid droplets regulates the inflammatory response in macrophages. PNAS 119 (12).

Wang, H., Bell, M., Sreenevasan, U., Hu, H., Liu, J., Dalen, K., Londos, C., Yamaguchi, T., Rizzo, M.A., Coleman, R., Gong, D., Brasaemle, D., Sztalryd, C., 2011. Unique regulation of adipose triglyceride lipase (ATGL) by perilipin 5, a lipid droplet-associated protein. J Biol Chem 286 (18), 15707–15715. https://doi.org/10.1074/jbc.M110.207779.

Wang, T., Qin, L., Liu, B., Liu, Y., Wilson, B., Eling, T.E., Langenbach, R., Taniura, S., Hong, J.S., 2004. Role of reactive oxygen species in LPS-induced production of prostaglandin E2 in microglia. J Neurochem 88 (4), 939–947. https://doi.org/10.1046/J.1471-4159.2003.02242.X.

Wu, J.W., Wang, S.P., Alvarez, F., Casavant, S., Gauthier, N., Abed, L., Soni, K.G., Yang, G., Mitchell, G.A., 2011. Deficiency of liver adipose triglyceride lipase in mice causes progressive hepatic steatosis. Hepatology 54 (1), 122–132. https://doi.org/10.1002/hep.24338.

Xu, T., Sheng, L., Guo, X., & Ding, Z. (2021). Free Fatty Acid Increases the Expression of NLRP3-Caspase1 in Adipose Tissue Macrophages in Obese Severe Acute Pancreatitis. *Digestive Diseases and Sciences 2021 67:6*, *67*(6), 2220–2231. doi: 10.1007/S10620-021-07027-W.

Zambusi, A., Novoselc, K.T., Hutten, S., Kalpazidou, S., Koupourtidou, C., Schieweck, R., Aschenbroich, S., Silva, L., Yazgili, A.S., van Bebber, F., Schmid, B., Möller, G., Tritscher, C., Stigloher, C., Delbridge, C., Sirko, S., Günes, Z.I., Liebscher, S., Schlegel, J., Ninkovic, J., 2022. TDP-43 condensates and lipid droplets regulate the reactivity of microglia and regeneration after traumatic brain injury. Nat Neurosci 25 (12), 1608–1625. https://doi.org/10.1038/S41593-022-01199-Y.

Zechner, R., Kienesberger, P.C., Haemmerle, G., Zimmermann, R., Lass, A., 2009. Adipose triglyceride lipase and the lipolytic catabolism of cellular fat stores. J Lipid Res 50 (1), 3–21. https://doi.org/10.1194/JLR.R800031-JLR200.